From ether to acid: A plausible degradation pathway of glycerol dialkyl glycerol tetraethers

From ether to acid: a plausible degradation pathway of glycerol dialkyl glycerol tetraethers

Xiao-Lei Liu [a, b, *], Daniel Birgel [c], Felix J. Elling [a, ♯], Paul A. Sutton [d], Julius S. Lipp [a], Rong Zhu [a, §], Chuanlun Zhang [e], Martin Könneke [a], Jörn Peckmann [c, f], Steven J. Rowland [d], Roger E. Summons [b], Kai-Uwe Hinrichs [a]

[a] Organic Geochemistry Group, MARUM Center for Marine Environmental Sciences and Department of Geosciences, University of Bremen, 28359 Bremen, Germany

[b] Department of Earth, Atmospheric, and Planetary Sciences, Massachusetts Institute of Technology, 77 Massachusetts Avenue, Cambridge, MA 02139-4307, USA

[c] Institute of Geology, University of Hamburg, 20146 Hamburg, Germany

[d] School of Geography, Earth and Environmental Sciences, University of Plymouth, Plymouth, Devon PL4 8AA, U.K.

[e] State Key Laboratory of Marine Geology, Tongji University, Shanghai 200092, China

[f] Department of Geodynamics and Sedimentology, Center for Earth Sciences, University of Vienna, 1090 Vienna, Austria

[♯] Present address, Harvard University, 20 Oxford St, Cambridge, MA 02138, USA

[§] Present address, ETH Zurich, Universitätsstrasse 16, 8092 Zürich, Switzerland

* Corresponding author, E-mail: xlliu@mit.edu

Abstract

Glycerol dialkyl glycerol tetraether (GDGT) are ubiquitous microbial lipids with extensive demonstrated and potential roles as paleoenvironmental proxies. Despite the great attention they receive, comparatively little is known regarding their diagenetic fate. Putative degradation products of GDGTs, identified as hydroxyl and carboxyl derivatives, were detected in lipid extracts of marine sediment, seep carbonate, hot spring sediment and cells of the marine thaumarchaeon *Nitrosopumilus maritimus*. The distribution of GDGT degradation products in environmental samples suggests that both biotic and abiotic processes act as sinks for GDGTs. More than a hundred newly recognized degradation products afford a view of the stepwise degradation of GDGT via 1) ether bond hydrolysis yielding hydroxyl isoprenoids, namely, GDGTol (glycerol dialkyl glycerol triether alcohol), GMGD (glycerol monobiphytanyl glycerol diether), GDD (glycerol dibiphytanol diether), GMM (glycerol monobiphytanol monoether) and bpdiol (biphytanediol); 2) oxidation of isoprenoidal alcohols into corresponding carboxyl derivatives and 3) chain shortening to yield C_{39} and smaller isoprenoids. This plausible GDGT degradation pathway from glycerol ethers to isoprenoidal fatty acids provides the link to commonly detected head-to-head linked long chain isoprenoidal hydrocarbons in petroleum and sediment samples. The problematic C_{80} to C_{82} tetraacids that cause naphthenate deposits in some oil production facilities can be generated from H-shaped glycerol monoalkyl glycerol tetraethers (GMGTs) following the same process, as indicated by the distribution of related derivatives in hydrothermally influenced sediments.

1. INTRODUCTION

Lipid biomarkers have the potential of providing valuable information regarding the composition of ancient ecosystems and paleoenvironmental conditions throughout most of the sedimentary record (e.g., Peters et al., 2004). For most of the frequently used biomarkers, such as steroids, hopanoids, pigments and their derivatives, the post-depositional structural transformations are rather well constrained (e.g., Mackenzie et al., 1982; Innes et al., 1997; Peters et al., 2004; Brocks and Schaeffer, 2008) and contribute to the foundation of the geological biomarker concept that links geomolecules to their biological precursors. An exception is the intensively studied group of isoprenoidal glycerol dialkyl glycerol tetraether (GDGT) lipids produced by Archaea. Despite their prominent use as molecular proxies for the reconstruction of paleoenvironmental conditions (e.g., Ingalls and Pearson, 2013; Schouten et al., 2013) and, in their intact polar form, for the ecology of extant archaeal communities (e.g., Lipp and Hinrichs, 2009; Liu et al., 2011; Meador et al., 2015; Yoshinaga et al., 2015), our understanding of their post-depositional behavior is fragmentary.

Three principal archaeal lipid categories are observed in environmental and geological samples: (i) intact polar lipids (IPL) as building blocks of the cellular membrane, consisting of a glycerolalkylether backbone and a polar headgroup which, in most instances is glycosidic (Sturt et al., 2004, Lipp and Hinrichs, 2009), (ii) the corresponding core glycerol alkyl ethers derived from hydrolytic cleavage of the polar headgroups on timescales of days to several tens of millennia, depending on depositional conditions and

72 enzymatic activity (Harvey et al., 1986; Xie et al., 2013), and (iii) degradation products
73 of core glycerol alkyl ethers that occur as hydrocarbons (Moldowan and Seifert, 1979),
74 alcohols (Schouten et al., 1998; Saito and Suzuki, 2010) and carboxylic acids (Meunier-
75 Christmann, 1988; Schouten et al., 2003; Birgel et al., 2008a).
76
77 The second group, i.e., the core lipids, is among the most extensively studied biomarker
78 class in the last decade (Ingalls and Pearson, 2013; Schouten et al., 2013), in particular
79 the GDGT derivatives. GDGTs accumulate in cold and moderately heated aquatic
80 sediments with seemingly little molecular alteration and remain intact in sediments over
81 tens of millions of years (e.g., Kuypers et al., 2001). GDGTs, including the bacterial non-
82 isoprenoidal types (Weijers et al., 2009; Liu et al., 2012b), are among the most prominent
83 lipids in marine sediments and soils. Their ubiquity and abundance result from both the
84 widespread distribution of their producing, largely uncultured, microbes and their
85 relatively high recalcitrance caused by the ether-linkages. Within the domain Archaea,
86 GDGTs are taxonomically widely distributed and probably produced by members of all
87 phyla (Pearson and Ingalls, 2013; Schouten et al., 2013).
88
89 Thermal diagenesis (Rowland, 1990) and hydrous pyrolysis (Pease et al., 1998)
90 experiments have shown the generation of isoprenoidal hydrocarbons from fresh archaeal
91 cultures. The exact fate of GDGTs is not clear, but they seem to be the most plausible
92 precursors of a wealth of compounds of putative archaeal origin found in thermally
93 mature formations. These compounds include head-to-head linked C_{32} to C_{40} isoprenoid
94 hydrocarbons in petroleum samples (Moldowan and Seifert, 1979), biphytanediols

(Schouten et al., 1998; Saito and Suzuki, 2010) and biphytanediacids (Meunier-Christmann, 1988; Birgel et al., 2008a) in recent sediments and rock samples of possibly diagenetic and/or biogenic origin; however these diols or diacids have never been detected in any archaeal cell extracts. Another group of recently discovered, widespread compounds includes a series of glycerol ether derivatives, the glycerol dibiphytanol diethers (GDDs; Knappy et al., 2012; Liu et al., 2012a). Although the occurrence of core GDDs and their glycosidic intact polar lipids in archaeal cell extracts suggests that they play a role in archaeal lipid biosynthesis (Liu et al., 2012a; Meador et al., 2014), a diagenetic contribution of these lipids in natural settings cannot be ruled out (e.g., Yang et al., 2014).

Another conspicuous compound series of putative archaeal origin are the so-called 'H-shaped' or 'ARN' C_{80}-C_{82} isoprenoidal tetracarboxylic acids found in certain petroleum types (Lutnaes et al., 2006, 2007) and believed to contribute significantly to the problematic naphthenate deposits formed during oil processing (e.g., Baugh et al., 2004; 2005). The archaeal lipids that are structurally related to the C_{80} tetraacids are 'H-shaped' glycerol monoalkyl glycerol tetraethers (H-GMGTs) found in thermophilic archaeal taxa (Morii et al., 1998; Schouten et al., 2008a), although H-GMGT-0 may also have non-thermophilic origins (Schouten et al. 2013). Whether the C_{80} tetraacids are degradation products of H-GMGTs or actually bio-surfactants directly synthesized by Archaea living in the crude oil remains ambiguous (Lutnaes et al., 2006, 2007). To date, isoprenoidal tetracarboxylic acids have not been detected in archaeal cells.

Based on the distribution patterns of newly identified series of GDGT degradation products in sedimentary samples (hydrothermally overprinted sediments from the Guaymas Basin and a hot spring in China, Miocene seep carbonates, and marine subsurface sediments), cell extracts and hydrolysis experiments, here we construct a precursor-product reaction network from GDGTs to alcoholic and carboxylic acid biphytane derivatives. Additionally, through the identification of five types of putative intermediates in the sediment from Guaymas Basin, we provide strong support for the hypothesis that isoprenoidal C_{80} to C_{82} tetraacids are derived from step-wise degradation of 'H-shaped' GMGTs.

2. MATERIALS and METHODS

2.1. Sample collection and preparation

N. maritimus strain SCM1 was grown aerobically at 28 °C and pH 7.5 in 8.5 l HEPES-buffered Synthetic Crenarchaeota Medium (1.5 mM NH_4Cl; Könneke et al., 2005; Martens-Habbena et al., 2009). The medium was inoculated with 5% of a mid-logarithmic phase pre-culture of *N. maritimus*. Biomass was harvested early and late in the growth phase as well as early and late in the stationary phase (one batch for each time-point) using cross-flow filtration (Elling et al., 2014). Purity of the culture was checked daily by phase contrast microscopy. Growth was monitored by measuring nitrite formation photometrically (Stickland and Parsons, 1972) and by counting 2% formaldehyde-fixed, SYBR Green I stained cells (Lunau et al., 2005) at the beginning

and the end of the experiment. Lipids were extracted from each batch following a modified Bligh and Dyer protocol as described previously (Sturt et al., 2004; Elling et al., 2014).

The Marmorito seep carbonate samples (Marmorito limestone; see also Peckmann et al., 1999) were taken close to the village of Marmorito, in the Monferrato hills close to Torino, Italy. The Marmorito limestone is composed of dolomite and calcite, and is embedded in Miocene strata chiefly consisting of siliciclastic sediments that were deposited in a marine shelf environment. Rock samples from the vicinity Marmorito, comprising not only the so-called Marmorito limestone, are among the early examples where methane-seepage, fossil chemosynthetic benthic communities, molecular fossils, and methane-related carbonate precipitation have been described (e.g., Clari et al., 1988, 1994; Peckmann et al., 1999; Thiel et al., 1999). Apart from the characteristic molecular fossils of the consortium mediating the anaerobic oxidation of methane, biomarkers of aerobic methanotrophic bacteria were also found (Peckmann et al., 1999; Birgel and Peckmann, 2008). A detailed list of compounds identified in the Marmorito limestone and a description of the applied decalcification procedure can be found in Birgel and Peckmann (2008) and references therein. Lipid extraction was performed as described in Birgel et al. (2006).

The Guaymas Basin sediment sample was retrieved during the *RV Atlantis* cruise AT15-56 to the Guaymas Basin, Gulf of California, Mexico, during *Alvin* dive 4568 (November 22 to December 6 2009, 27° 00.449’ N, 111° 24.347’ W). The sample came from an oil-

164 impregnated hydrothermally active area, where sedimentary temperature steeply
165 increased from ~3 °C to ~100 °C within 35 cm (Gutierrez et al., 2015). The sample was
166 surface sediment (0-4 cm depth) with the highest temperature at time of sampling
167 reaching ~12 °C. However, due to the dynamic nature of the hydrothermal activity and
168 the upward flux of fluids in the Guaymas Basin (Pearson et al., 2005), it is likely that the
169 sample has been previously heated to higher temperatures and/or contains extractable
170 organic matter formed in deeper layers at higher temperatures. Wet sediment (15-20 g)
171 was extracted using the modified Bligh and Dyer method (Sturt et al., 2004). To
172 minimize the heavy background of oil contaminants, an aliquot of the total lipid extract
173 (TLE) was cleaned with the Hybrid SPE®-Phospholipid cartridges before LC-MS
174 analysis according to the method described by Zhu et al. (2013a).
175
176 Two further sediment samples, including a marine subsurface sediment (Leg201-1227;
177 Hole 1227A, mixed from five samples: 1227A-2H2-65-75cm, 1227A-2H5-83-93cm,
178 1227A-3H2-55-65cm, 1227A-11H2-118-128m, 1227A-13H3-0-15cm; spanning from
179 8.1-113.6 m below sea floor) and a hot spring sediment (T-15, see sample description in
180 SI) were also extracted with the Bligh and Dyer method for lipid analysis.
181
182 **2.2. Lipid analysis**
183
184 For lipid analysis by normal phase liquid chromatography (NP-LC), an aliquot of TLE of
185 each sample was dissolved in *n*-hexane/isopropanol (99.5:0.5 v/v) for injection.
186 Compound separation was performed on a Dionex Ultimate 3000 RS UHPLC system

187 (Thermo Scientific, Bremen, Germany) at 50 °C, following the recently developed
188 tandem column protocol (Becker et al., 2013) using two ACQUITY UPLC® BEH Hilic
189 Amide columns (2.1 x 150 mm, 1.7 µm, Waters). Solvent gradient was programmed for a
190 constant flow rate of 0.5 mL min^{-1} and a linear increase from 3% B to 20% B in 20
191 minutes, and then linearly to 50% B at 35 minutes, after then up to 100% B at 45 min,
192 holding for 6 minutes, finally back to 3% B for 9 minutes to re-equilibrate the column,
193 where A was *n*-hexane and B was *n*-hexane/isopropanol (90:10). Detection was achieved
194 with a Bruker Maxis accurate-mass quadrupole time-of-flight (qTOF) mass spectrometer
195 (Bruker Daltonik, Bremen, Germany) coupled to the UHPLC via an atmospheric pressure
196 chemical ionization (APCI) interface run in positive ion mode. APCI source parameters
197 were as follows: corona current 3500 nA, nebulizer gas pressure 5 bar, drying gas flow 8
198 L min^{-1}, drying gas (N_2) temperature 160 °C, vaporizer temperature 400 °C. The scan
199 range was 150-2000 m/z at a rate of 2 Hz. Lipids were identified based on accurate mass
200 (better than 1 ppm), retention times and diagnostic fragments and under consideration of
201 general GDGT mass spectral features (e.g., Liu et al., 2012b), and quantified by
202 measurement of $[M+H]^+$ responses, with a extraction window of individual ion
203 chromatograms of ± 0.01 *m/z* units.
204
205 For the detection of carboxylic acid derivatives, reversed phase (RP) LC-MS (cf. Zhu et
206 al., 2013b) was applied with the same LC system using an ACE3 C_{18} column (2.1 × 150
207 mm, 3 µm; Advanced Chromatography Technologies Ltd., Aberdeen, Scotland) coupled
208 with a guard cartridge and maintained at 45 °C, and the same mass spectrometer (qTOF)
209 equipped with an electrospray ionization (ESI) source and operated in positive mode

(Bruker Daltonik, Bremen, Germany). An aliquot of TLE of each sample was dissolved in methanol prior to injection. Separation of compounds was achieved isocratically with 100% eluent A for 10 min, followed by a rapid gradient to 24% B in 5 min, and then a slow gradient to 65% B in 55 min at a flow rate of 0.2 mL min^{-1}, where the eluent A was methanol/formic acid/14.8 M NH_{3aq} (100:0.04:0.10, v/v/v) and B was 2-propanol/formic acid/14.8 M $NH_{3(aq)}$ (100:0.04:0.10, v/v/v). After each run, the column was washed with 90% B for 10 min and subsequently re-equilibrated with 100% A for another 10 min. The ESI-MS conditions were set as capillary voltage 4500 V, nebulizing gas (N_2) pressure 0.8 bar, and dry gas (N_2) 4 L min^{-1} at a temperature of 200 °C.

3. RESULTS

3.1. Structural elucidation of products of GDGT breakdown

Table 1 provides an overview of 19 distinct compound classes observed in this study. Structural assignments are based on formulae established from accurate mass measurements, chromatographic behavior and tandem mass spectrometry (MS^2) (Fig. 1, 2 and 3 and S1a-d contain data showing detailed MS^2 fragmentation patterns). Many compounds remain only tentatively identified. Identifications of the hydroxyl derivatives, including GDGTol (glycerol dialkyl glycerol triether alcohol), GMGD (glycerol monobiphytanyl glycerol diether), GDD (glycerol dibiphytanol diether), GMM (glycerol monobiphytanol monoether) and bpdiol (biphytanediol), were additionally confirmed by examination of products released after acidic degradation of purified GDGT-0

233 (compound compositions are given in Fig. S2). The identification of the H-tetrol was
234 additionally supported by the co-injection of an H-tetrol mixture synthesized by reduction
235 of the corresponding acids, which were isolated and characterized by NMR spectroscopy
236 previously (Lutnaes et al., 2007; Fig. S3, preparation described in SI). C_{39} isoprenoids
237 were assigned based on chromatographic behavior, molecular formulae generated from
238 accurate mass measurements and characteristic fragment ions (MS^2 fragmentation
239 patterns are shown in Fig. S1a). For example, the two isomers of GDGTol-0 (highlighted
240 with green circles in Fig. 3e) eluted earlier than those of $C_{40/39}$-GDGTA-0 (two pink solid
241 line circles in Fig. 3e). In addition, GDGTol-0 and $C_{40/39}$-GDGTA-0 also have
242 measurably different molecular masses, $[M+H]^+$ of m/z: 1320.3312 and 1320.2930,
243 respectively and these afford calculated formulae of $C_{86}H_{175}O_7^+$ for GDGTol-0 and
244 $C_{85}H_{171}O_8^+$ for $C_{40/39}$-GDGTA-0. To add weight to this assignment, the fragment ion of
245 m/z: 651.6245 in the MS^2 of $C_{40/39}$-GDGTA-0 compared to m/z: 665.6391 of GDGTA-0
246 represents the loss of methylene from the biphytane (Fig. S1a).
247
248 **3.2. Terminally hydroxylated biphytanyl derivatives**
249
250 Hydrolysis of the glycerol ether bonds in isoprenoidal GDGT generates five types of
251 biphytane-based alcohols, with and without the glycerol backbones, namely, GDGTol,
252 GMGD, GDD, GMM and bpdiol (compound structures are given in Fig. S2). For
253 example, we demonstrate their structural relationships to acyclic caldarchaeol, GDGT-0,
254 with a parallel glycerol configuration, a distribution observed in a seep carbonate sample
255 from Marmorito (Fig. 1a and b). Constitutional isomers, which are labeled as peak ‘a’

256 and ‘b’ in the chromatogram of GDGTol, GMGD and GMM in Fig. 1, represent different
257 combinations of *sn*-2 or *sn*-3 glycerol ether bonding. Degradation products of the ring-
258 containing GDGTs are more numerous, due to different possible arrangements of a ring
259 on the biphytanyl chains. A detailed isomeric study of GDGTol, GMGD and GMM and
260 their implications will be discussed in our following works. As for H-GMGTs, which
261 have two biphytane chains linked by a bis-methylene C-C bond at position C_{20} (Lutnaes
262 et al., 2006; 2007) the cleavage of two glycerol units results in a C_{80} H-tetrol, instead of
263 two biphytanediols (bpdiols). These hydroxyl derivatives of GDGT were either all, or at
264 least some, present in our sample set comprising extracts of marine sediment, seep
265 carbonate, hydrothermal vent, hot spring sediment and archaeal cell extract (Table 1).
266
267 **3.3. Terminally-carboxylated biphytanyl derivatives**
268
269 Carboxylic acids, corresponding to each of hydroxyl derivatives mentioned above, could
270 logically be generated by oxidation of each terminal alcohol of the biphytane. These were
271 also detected in the analyzed samples and are subsequently referred to as GDGTA for the
272 carboxyl analogue of GDGTol and GMMA for GMM (Fig. 1a, b and Table 1). For
273 isoprenoids possessing two primary hydroxyl groups, such as GDD and bpdiol, both
274 mono- and dicarboxyl analogues were detected, with the monocarboxyl derivative of
275 GDD termed GDDA, the dicarboxyl derivative GDDAA, as well as biphytane mono- and
276 diacids. In the case of GMGD, which does not possess a primary biphytane-bound
277 hydroxyl group, no acid derivatives were detected. In the case of H-tetrol, which contains
278 four primary hydroxyl groups on its two linked bpdiols, we detected mono-, di-, tri- and

tetraacids in an oily sediment sample collected from a hydrothermal vent site in Guaymas Basin (Fig. 2).

Under APCI conditions, the ionization patterns of biphytane monoacid/monool (bpmonoacid/ol) and biphytanediacids (bpdiacid) differed from bpdiols. A protonated molecular ion $[M+H]^+$ was usually the major ion in mass spectra of bpdiols, while the acids produced more complex mass spectra in our analyses. Dehydrated molecular ions and unknown adducts were formed during the ionization of carboxyl derivatives (Fig. 1b and S1d). The main adduct ions detected were $[M+H+42]^+$ for bpmonoacid/ol and $[M+H+84]^+$ for bpdiacids (Fig. S1d).

3.4. C_{39} and C_{38} isoprenoids

In addition to the series of hydroxylated and carboxylated C_{40} biphytane derivatives, we identified some with shortened alkyl chains such as the C_{39} analogues. For example, in most analyzed samples analogues with one methylene unit less than GDGTol and GDGTA, here termed $C_{40/39}$-GDGTol and $C_{40/39}$-GDGTA (Arabic numbers represent the carbon number of the two isoprenoidal chains in the molecule), always co-occurred at lower abundance with their $C_{40/40}$ analogues (Fig. 3b, e). C_{39} derivatives were also detected as analogues of GDD, bpdiol and GMM (Fig. 3a, c and d). Additionally, we detected signals that we attribute to the pseudo-homologue of C_{38} isoprenoids, as GDGTol and GDD (Fig. 3a and b). Within the group of GDDs reduced by two C-atoms, we observed both $C_{39/39}$ and $C_{40/38}$ derivatives (Fig. 3a). Three isomers of the acyclic and

four isomers of crenarchaeol-related GDD were detected (Fig. 3a). In previous studies $\delta^{13}C$ depleted C_{39} head-to-head linked isoprenoids were detected in Cretaceous (Sandy et al., 2012) and Carboniferous seep carbonates (Birgel et al., 2008b); those compounds presumably represent the hydrocarbon derivatives of the C_{39} functionalized compounds found in this study. Interestingly, no derivatives of C_{80} H-tetrol and tetraacid with reduced carbon chains were detected in our samples.

4. DISCUSSION

4.1. The occurrence of GDGT degradation derivatives in environmental samples

The distributions of major degradation derivatives of GDGT-0 and H-GMGT-0 were compared in four representative environmental samples (Fig. 4), which include modern to late Miocene marine subsurface sediment (Leg201-1227), modern hot spring (T-15) and hydrothermally heated sediment (Guaymas Basin 4568), and the Miocene Marmorito seep carbonate. Distinct patterns of degradation derivatives in these four types of samples from different environments and of different age (modern sediments and ancient carbonate rock) reflect variable degrees of degradation and preservation.

4.1.1. Distributions of regular GDGT degradation products in environmental samples

The distributions of GDGT degradation products across our sample set suggest that the biological sources of GDGTs, as well as the debris depositional histories, influence the

325 diagenetic trajectory of GDGTs. By way of example, the degradation derivatives of
326 GDGT-0 are around twice as abundant as their precursor in the marine sediment sample
327 of Leg 201-1227, in which bpdiol-0 comprises over half of all of the detected degradation
328 products (Fig. 4). However, the GDGT degradation derivatives in Miocene seep
329 carbonates exhibited a lower overall relative abundance, but with a greater variety and
330 portion of labile components, such as the carboxyl derivatives (Table 1 and Fig. 4).
331 Regular isoprenoidal GDGTs (as compared to H-GMGTs) preserved in marine sediments
332 are primarily derived from planktonic archaea, dwelling in the water column. In contrast,
333 those in seep carbonates receive a larger *in-situ* contribution from benthic communities
334 engaged in anaerobic oxidation of methane (AOM), as confirmed by low $\delta^{13}C$ values of
335 biphytanic diacids (cf. Birgel et al., 2008a). The higher proportion of degradation
336 derivatives compared to their GDGT precursors in deep subsurface sediment apparently
337 results from a mild to moderate degradation process, but degradation lasted longer than at
338 the Marmorito seep site and was favored by extensive transportation. The extraordinarily
339 good preservation of labile compounds in seep carbonates can be attributed to significant
340 *in-situ* GDGT production combined with co-eval carbonate formation and resulting early
341 lithification within methane seepage systems (e.g., Peckmann et al., 1999; Birgel et al.,
342 2008a), rather than representing a time-integrated pattern with input from various
343 sedimentary or sedimentary/planktonic archaea (cf. Feng et al., 2014; Birgel et al., 2008a).
344
345 The relative abundance of degradation products in Guaymas basin sediment is over 40%
346 of all GDGT-derived compounds (Fig. 4). Both biodegradation and thermal diagenesis
347 can be potential sources of degradation products, due to the presence of both active

348 microbial communities and high temperature hydrothermal fluids in Guaymas basin
349 sediments (Teske et al., 2014; Gutierrez et al., 2015). In contrast, there are only low
350 abundances of GDD and bpdiol (< 10%) detected as GDGT degradation products in the
351 hot spring sediment (Fig. 4).
352
353 In addition to the contrasting patterns of the different environments, there is a
354 compositional discrepancy between each class of GDGT product within the same sample.
355 For example, previous studies that documented the presence of bpdiols and bpdiacids in
356 environmental samples have shown that the ring distributions and carbon isotopic
357 compositions differ for biphytanes released from coexisting GDGTs (Schouten et al.,
358 1998; Birgel et al., 2008a; Saito and Suzuki, 2010). The Marmorito limestone samples
359 (Fig. 5; Birgel et al. (2008a) provide results on hydrocarbons and bpdiacids), show
360 distinct ring distribution patterns for GDGT, bpdiol, bpmonoacid/ol and bpdiacid;
361 GDGTs are dominated by GDGT-0 and crenarchaeol, while the relative abundance of
362 tricyclic biphytane derivatives derived from crenarchaeol gradually decreases for the
363 hydroxyl to carboxyl products. Multiple inputs, combined with selective preservation
364 could cause such distributional differences. The ring distribution of GDGTs preserved in
365 sediments may reflect a mixed contribution from both planktonic and benthic species and
366 is frequently dominated by compounds from planktonic sources (Wuchter et al., 2005;
367 Huguet et al., 2007; Lengger et al., 2012). Planktonic and sedimentary archaeal
368 communities could contribute different lipids. Further, compared to biphytanyl products
369 derived from benthic species within the sediment, those derived from water column will
370 have experienced a very different transportation history. This might explain why the

371 tricyclic diacid derived from planktonic archaea are rare, while the acyclic, mono- and
372 bicyclic diacids with origins from sedimentary methanotrophic archaea, are more
373 common and more ^{13}C-depleted in the seep carbonate (isotopic data published in Birgel
374 et al., 2008a).
375
376 ***4.1.2. The degradation of H-GMGTs to H-tetrols and H-tetraacids***
377
378 H-GMGT-0 and its hydroxylated degradation products are generally present in the
379 samples from low-temperature and hydrothermal environments (Table 1 and Fig. 4),
380 while compounds with multiple cycloalkyl groups and additional methylations are
381 restricted to the hydrothermal samples alone. In low-temperature samples, H-GMGT-0 is
382 far more abundant than H-GMD-0 (acyclic H-shaped glycerol monoalkyl diether) and
383 tetrol-0 (Fig. 4). The apparently different patterns of H-GMGT-0 and its derivatives,
384 compared to GDGT-0 and its highly abundant degradation products, point to
385 contributions of distinct species and/or different diagenetic pathways.
386
387 We detected H-tetrol and H-tetraacids, and their partially oxidized 'H-shaped' mono-, di-
388 and triacid intermediates, in the oily Guaymas Basin sediment (Fig. 2). The detection of
389 these intermediates likely implies enzymatic modification of existing 'H-shaped' GDGTs
390 by living organisms. H-tetraacids accumulated in naphthenate deposits in oil well
391 infrastructure and pipelines and in crude oils, have distributions usually dominated by 4-8
392 cyclopentyl rings and 1 or 2 additional methyl substitutions (Lutnaes et al., 2007; Sutton
393 & Rowland, 2014). Although H-GMGT-0 is known to be present in a broad range of

394 mesophilic environments (Schouten at al., 2008a), those with multiple cyclizations and
395 methylations have been only detected in hyperthermophilic archaeal species (Schouten et
396 al., 2008b; Knappy et al., 2011; Liu et al., 2012b). H-GMGTs existed in both hot spring
397 and Guaymas Basin sediments analyzed. However, H-tetraacids were only found in the
398 oil-impregnated Guaymas Basin sediment (Table 1). In addition to the diagenetic
399 contribution, Lutnaes et al. (2006) also speculated that these tetraacids might be produced
400 by thermophilic, oil-degrading archaea as biosurfactants to facilitate their metabolism.
401 Additional studies would be required to test this rigorously. Given the occurrence of
402 biphytane, C_{39} and smaller head-to-head linked isoprenoids in the geological record, C_{80}
403 based H-shaped isoprenoidal hydrocarbons might also exist. Whilst these are not
404 detectable with conventional GC-MS, they would be amenable to high temperature GC-
405 MS (cf. Sutton & Rowland, 2012)
406
407 **4.2. The occurrence of GDGT degradation derivatives in archaeal cell extracts**
408
409 In a previous study concerning the characterization of GDD, Liu et al. (2012a) observed
410 the existence of core GDD in the cell extracts of the methanogen *Methanothermococcus*
411 *thermolithotrophicus*. More recently, Meador et al. (2014) reported detection of both
412 core and monoglycosidic GDD (1G-GDD) in a culture of the planktonic ammonia
413 oxidizer *N. maritimus*. Here we extend these observations and report newly identified
414 biphytane derivatives in fresh biomass collected at different growth phases of cell
415 extracts of the archaeon *N. maritimus*. Core lipids accounted for 8.2-15% of the total
416 detected lipids during different growth phases (Elling et al., 2014). We selected the most

417 abundant component, crenarchaeol, to illustrate the distribution of its hydroxyl and
418 carboxyl derivatives in different growth phases. GDD-Cren. and bpdiol-Cren. were the
419 only detected hydroxyl components during early exponential growth (Fig. 6); they jointly
420 accounted for less than 1% of all crenarchaeol-based derivatives. In the late growth phase,
421 however, the relative abundances of GDD-Cren. and bpdiol-Cren. were almost doubled,
422 while the acid (GDDA-Cren.) and a C_{39} component ($C_{40/39}$-GDD-Cren.) emerged as well.
423 GDD-Cren., depleted by two methylene units ($C_{39/39}$ and $C_{40/38}$-GDD-Cren.), together
424 with GDGTol-Cren. were only observed in the stationary phase.
425
426 Although these derivatives occurred in cell extracts, they cannot be simply attributed as
427 intermediates of GDGT biosynthesis. For example, the carboxyl and C_{39} based
428 derivatives, such as GDDA and $C_{40/39}$-GDD, are more likely further oxidized products of
429 GDD. For example, archaeal biphytanyl moieties, synthesized via the mevalonic acid
430 (MVA) or methylerythritol phosphate (MEP) pathways, should have a carbon number
431 that is a multiple of five. Accordingly, the most plausible formation pathway for the C_{38}
432 and C_{39} moieties is oxidation and decarboxylation of C_{40} precursors. Formation of C_{38}
433 and C_{39} moieties via degradation of C_{40} biphytanyl moieties is also consistent with the
434 higher relative abundance of GDDA and $C_{40/39}$-GDD during the late stationary phase (Fig.
435 6). The loss of one methylene unit represents an α-oxidation step. A similar well-known
436 enzymatic α-oxidation of isoprenoids is that of phytanic acid (C_{20}) to pristanic acid (C_{19})
437 by a wide range of organisms (e.g., Rontani and Volkman, 2003; Jansen and Wanders,
438 2006, and other studies cited therein). As in phytanic acid, the C_3 methyl group in
439 biphytanic acid (C_{40}) derivatives prevents an initial β-oxidation mechanism; instead,

these compounds undergo α-oxidation to yield C_{39} based carboxyl isoprenoids. In such a scenario the production of GDD and GDGTol consisting of C_{38} derivatives would require two successive α-oxidation steps. This is inconsistent with the reported α-oxidation of phytanic acid, which is followed by hydroxylation and then β-oxidation (e.g. Jansen and Wanders, 2006, and other studies cited therein). Therefore, elucidation of the degradation process leading to a C_{38} isoprenoid requires further study. Furthermore, α- as well as β-oxidation would only result in carboxyl derivatives, and could not explain the occurrence of hydroxyl analogues, such as $C_{40/39}$-GDD and $C_{40/39}$-GDGTol (Fig. 3). Although the detection of carboxyl derivatives and C_{38} and C_{39} based isoprenoids in a metabolic active culture of *N. maritimus* may imply an intracellular modification of existing C_{40} based lipids, probably as a result of cell senescence, their contribution is less than 2% of the core lipid fraction, or approximately 0.01% of the entire lipidome. The exact mechanisms responsible for the remarkable proportions (up to 70% in the marine subsurface sediment, Leg201-1227, Fig. 4) of degradation products in environmental samples remain unresolved. The presence of degradation products in archaeal cell extracts, as well as their increase towards later growth and stationary phases, suggests that some are formed rapidly and probably via enzymatic catalysis. On the other hand, the high proportion and diversity of degradation products in the hydrothermally influenced settings also leaves room for an additional role of abiotically-mediated chemical degradation reactions, at least for some of the speculated steps leading via catagenesis from GDGTs to biphytanyl hydrocarbons (cf. Rowland, 1990).

4.3. Evidence of analogous behavior of non-isoprenoidal GDGTs

463 Non-isoprenoidal GDGTs, such as the hybrid isoprenoidal/branched GDGT (IB-GDGT)
464 and branched GDGTs, are known to be widely distributed in various environments,
465 although their exact structures and biological source(s) remain unknown (Liu et al.,
466 2012b). The degradation pathways described here are not limited to archaeal GDGTs. For
467 example, in one of the seep carbonate samples, which contains high abundances of
468 branched and IB-GDGTs, there are non-isoprenoidal GDDs, GMMs and diols detected.
469 These possibly represent degradation products of the branched and IB-GDGTs in the
470 same deposit (Fig. S4 and S5). Our analytical methods also reveal the presence of
471 carboxyl derivatives of these lipids. Non-isoprenoidal GDGTol, GDGTA, GMGD, and
472 their corresponding products with reduced carbon chains (loss of one or two methylene
473 units) were not identified, however, and we attribute this to their low overall abundance
474 in the analyzed samples.
475

476 ## 5. CONCLUSIONS

477

478 As with other lipid classes, the intact archaeal tetraethers released from the cells of
479 defunct archaea into various depositional settings, are subjected to diagenesis in
480 sediments. We detected three major classes of GDGT degradation products comprising
481 biphytanyl molecules with terminal hydroxyl, terminal carboxyl and shortened carbon
482 chains. A hypothetical scheme of the GDGT degradation pathway to rationalize such a
483 pathway is illustrated in Fig. 7. The labile polar head groups of intact GDGTs, as they
484 occur in living cells, are initially lost to produce the more recalcitrant core GDGTs.
485 Hydrolysis of the different ether bonds then, as we suggest, results in discrete series of

hydroxyl derivatives composed of one or two glycerol and biphytanol units. Oxidation of each terminal hydroxyl functional group may then generate related carboxyl products. Elimination of the C_1 carbon via α-oxidation and subsequent β-oxidation steps, will likely convert the C_{40} biphytanyl based compounds into shortened isoprenoids, such as $C_{40/39}$-GDGTA and $C_{40/39}$-GDGTol. Further chemical or biological alteration of these intermediates may over geological time, result in the C_{40}, C_{39} and smaller head-to-head linked isoprenoidal hydrocarbons reported to occur in petroleum and marine deposits (e.g. Moldowan and Seifert, 1979; Birgel et al., 2008b).

A multitude of diagenetic processes will lead to the degradation of GDGTs in sediments. However, we also observed the accumulation of C_{39} based carboxyl isoprenoids in the later growth and stationary phases of an archaeal cell culture. This implies that enzymatic pathways for degradation of GDGTs also exist, very likely, as a response to substrate limitation, senescence or cell lysis. Additional studies will be required to study this facet in greater detail.

The detection of H-GMGT, H-GMD, H-tetrols and their further oxidized carboxyl intermediates in the oil-contaminated sediments of Guaymas Basin (Fig. 2) elucidated a formation pathway from H-GMGT to H-tetraacids under anoxic conditions. Metagenomic data for samples from the Guaymas Basin and especially sediment with oil impregnation may help to elucidate the origin of H-tetraacids further.

508 In various geological settings these hydroxyl and carboxyl derivatives co-occur with their
509 GDGT precursors, including both isoprenoidal and non-isoprenoidal GDGTs. Our
510 analysis of their distributions in environmental samples and archaeal cell extracts
511 represents an initial effort to document the possible diagenetic pathways of GDGTs and
512 to bring about the same level of understanding that we have for steroids and triterpenoids
513 (e.g., Peters et al., 2004).
514

ACKNOWLEDGEMENTS

X.-L.L. was funded by European Union's Seventh Framework Programme–"Ideas" Specific Programme, ERC grant agreement No. 247153 (Advanced Grant DARCLIFE; PI K.-U.H.), the Simons Foundation Collaboration on the Origins of Life (SCOL). Cultivation experiments and lipid analyses at the University of Bremen were funded by the Deutsche Forschungsgemeinschaft through the Gottfried Wilhelm Leibniz Prize awarded to K.-U.H. (Hi 616-14-1). SJR and PAS were funded by a European Research Council Advanced Investigators Award to SJR for project OUTREACH (agreement no. 228149).

529 **REFERENCES**

530

531 Baugh T.D., Wolf N.O., Mediaas H., Vindstad J.E., Grande K. (2004) Characterization of
532 a Calcium Naphthanate Deposit -The ARN Acid Discovery. Preprints/American
533 Chemical Society, Division of Petroleum Chemistry **49**, 274−276.

534 Baugh T.D., Grande K.V., Mediaas H., Vindstad J.E., Wolf N.O. (2005) In The
535 Discovery of High Molecular Weight Naphthenic Acids (ARN Acid) Responsible for
536 Calcium Naphthenate Deposits. SPE International Symposium on Oilfield Scale,
537 Aberdeen, U.K., May 11−12 2005; SPE 93011.

538 Becker K.W., Lipp J.S., Zhu C., Liu X.-L., Hinrichs K.-U. (2013) An improved method
539 for the analysis of archaeal and bacterial ether core lipids. *Org. Geochem.* **61**, 34-44.

540 Birgel, D., Thiel, V., Hinrichs, K.-U., Elvert, M., Campbell, K.A., Reitner, J., Farmer,
541 J.D., Peckmann, J. (2006) Lipid biomarker patterns of methane-seep microbialites
542 from the Mesozoic convergent margin of California. *Org. Geochem.* **37**, 1289–1302.

543 Birgel, D., Peckmann, J. (2008) Aerobic methanotrophy at ancient marine methane seeps:
544 a synthesis. *Org. Geochem.* **39**, 1659–1667.

545 Birgel D., Elvert M., Han X., Peckmann J. (2008a) ^{13}C-depleted biphytanic diacids as
546 tracers of past anaerobic oxidation of methane. *Org. Geochem.* **39**, 152–156.

547 Birgel, D., Himmler, T., Freiwald, A., Peckmann, J. (2008b) A new constraint on the
548 antiquity of anaerobic oxidation of methane: Late Pennsylvanian seep limestones
549 from southern Namibia. *Geology* **36**, 543–546.

550 Brocks J.J., Schaeffer P. (2008) Okenane, a biomarker for purple sulfur bacteria
551 (Chromatiaceae), and other new carotenoid derivatives from the 1640 Ma Barney
552 Creek Formation. *Geochim. Cosmochim. Acta* **72**, 1396–1414.

553 Clari P., Gagliardi C., Governa M.E., Ricci B., Zuppi G.M. (1988) I calcari de
554 Marmorito: Una testimonianza di processidiagene- tici in presenza di metano. *Boll*
555 *Museo Regionale Sci Naurali Torino* **6**, 197–216.

556 Clari P., Fornara L., Ricci B., Zuppi G.M. (1994) Methane-derived carbonates and
557 chemosymbiotic communities of Piedmont (Miocene, northern Italy): an update.
558 *Geo-Marine Lett.* **14**, 201–209.

559 Elling F.J., Könneke M., Lipp J.S., Becker K.W., Gagen E.J., Hinrichs K.-U. (2014)
560 Effects of growth phase on the membrane lipid composition of the thaumarchaeon
561 *Nitrosopumilus maritimus* and their implications for archaeal lipid distributions in
562 themarine environment. *Geochim. Cosmochim. Acta* **141**, 579–597.

563 Gutierrez, T., Biddle, J.F., Teske, A., Aitken, M.D. (2015) Cultivation-dependent and
564 cultivation-independent characterization of hydrocarbon-degrading bacteria in
565 Guaymas Basin sediments. *Front. Microbiol.* **6**, doi: 10.3389/fmicb.2015.00695

566 Harvey, H.R., Fallon, R.D., Patton, J.S. (1986) The effect of organic matter and oxygen
567 on the degradation of bacterial membrane lipids in marine sediments. *Geochim.*
568 *Cosmochim. Acta* **50**, 795–804.

569 Huguet, C., Schimmelmann, A., Thunell, R., Lourens, L.J., Sinninghe Damsté, J.S.,
570 Schouten, S. (2007) A study of the TEX_{86} paleothermometer in the water column and
571 sediments of the Santa Barbara Basin, California. *Paleoceanography* **22**,
572 doi:10.1029/2006PA001310

573 Innes, H.E., Bishop, A.N., Head, I.M., Farrimond, P. (1997) Preservation and diagenesis
574 of hopanoids in Recent lacustrine sediments of Priest Pot, England. *Org. Geochem.*
575 **26**, 565-576.

576 Jansen G.A., Wanders R.J.A. (2006) Alpha-Oxidation. *Biochim Biophys Acta – Mol. Cell*
577 **1763**, 1403–1412.

578 Könneke M., Bernhard A. E., de la Torre J. R., Walker C. B., Waterbury J. B., Stahl D.
579 A. (2005) Isolation of an autotrophic ammonia-oxidizing marine archaeon. *Nature*
580 **437**, 543–546.

581 Knappy, C.S., Nunn, C.E.M., Morgan, H.W., Keely, B.J. (2011) The major lipid cores of
582 the archaeon *Ignisphaera aggregans*: implications for the phylogeny and
583 biosynthesis of glycerol monoalkyl glycerol tetraether isoprenoid lipids.
584 *Extremophiles* **15**, 517–528.

585 Knappy C.S., Keely B.J. (2012) Novel glycerol dialkanol triols in sediments:
586 transformation products of glycerol dibiphytanyl glycerol tetraether lipids or
587 biosynthetic intermediates? *Chem. Commun.* **48**, 841–843.

588 Kuypers, M. M. M., Blokker, P., Erbacher, J., Kinkel, H., Pancost, R. D., Schouten, S. and
589 Sinninghe Damsté, J. S. (2001) Massive expansion of marine Archaea during a
590 mid-Cretaceous oceanic anoxic event. *Science* **293**, 92-95.

591 Lengger, S.K., Hopmans, E.C., Reichart, G.-J., Nierop, K.G.J., Damsté, J.S.S., Schouten,
592 S. (2012) Intact polar and core glycerol dibiphytanyl glycerol tetraether lipids in the
593 Arabian Sea oxygen minimum zone. Part II: Selective preservation and degradation
594 in sediments and consequences for the TEX_{86}. *Geochim. Cosmochim. Acta* **98**, 244–
595 258.

596 Lipp J.S., Hinrichs K.-U. (2009) Structural diversity and fate of intact polar lipids in
597 marine sediments. *Geochim. Cosmochim. Acta* **73**, 6816–6833.

598 Liu, X.-L., Lipp, J.S., Hinrichs, K.-U. (2011) Distribution of intact and core GDGTs in
599 marine sediments. *Org. Geochem.* **42**, 368–375.

600 Liu X.-L., Lipp J.S., Schröder J.M., Summons R.E., Hinrichs K.-U. (2012a) Isoprenoid
601 glycerol dialkanol diethers: A series of novel archaeal lipids in marine sediments.

602 *Org. Geochem.* **43**, 50–55.

603 Liu X.-L., Summons R.E., Hinrichs K.-U. (2012b) Extending the known range of
604 glycerol ether lipids in the environment: structural assignments based on tandem
605 mass spectral fragmentation patterns. *Rapid Commun. Mass Spectrom.* **26**, 2295–
606 2302.

607 Lunau M., Lemke A., Walther K., Martens-Habbena W., Simon M. (2005) An improved
608 method for counting bacteria from sediments and turbid environments by
609 epifluorescence microscopy. *Environ. Microbiol.* **7**, 961–968.

610 Lutnaes B.F., Brandal Ø., Sjöblom J., Krane J. (2006) Archaeal C_{80} isoprenoid tetraacids
611 responsible for naphthenate deposition in crude oil processing. *Org. Biomol. Chem.* **4**,
612 616.

613 Lutnaes B.F., Krane J., Smith B.E., Rowland S.J. (2007) Structure elucidation of C_{80}, C_{81}
614 and C_{82} isoprenoid tetraacids responsible for naphthenate deposition in crude oil
615 production. *Org. Biomol. Chem.* **5**, 1873.

616 Mackenzie, A.S., Brassell, S.C., Eglinton, G., Maxwell, J.R. (1982) Chemical fossils –
617 the geological fate of steroids. *Science* **217**, 491–504.

618 Martens-Habbena W., Berube P.M., Urakawa H., de la Torre J.R., Stahl D.A. (2009)
619 Ammonia oxidation kinetics determine niche separation of nitrifying Archaea and
620 Bacteria. *Nature* **461**, 976–979.

621 Meador T.B., Zhu C., Elling F.J., Könneke M., Hinrichs K.-U. (2014) Identification of
622 isoprenoidglycosidic glycerol dibiphytanoldiethers and indications for their
623 biosynthetic origin. *Org. Geochem.* **69**, 70–75.

624 Meador, T.B., Bowles, M., Lazar, C., Zhu, C., Teske, A., Hinrichs, K.-U. (2015) The
625 archaeal lipidome in estuarine sediment dominated by members of the Miscellaneous
626 Crenarchaeotal Group. *Environ. Microbiol.* **17**, 2441-2458.

627 Meunier-Christman C. (1988) Geochimie organique de phosphates et schistes bitumineux
628 marocains: etude du processus de phosphatogenese. PhD thesis, University of
629 Strasbourg, p. 133.

630 Moldowan J.M., Seifert W.K. (1979) Head-to-head linked isoprenoid hydrocarbons in
631 petroleum. *Science* **204**, 169–171.

632 Morii, H., Eguchi, T., Nishihara, M., Kakinuma, K., König, H., Koga, Y. (1998) A novel
633 ether core lipid with H-shaped C_{80}-isoprenoid hydrocarbon chain from the
634 hyperthermophilic methanogen *Methanothermus fervidus*. *Biochim. Biophys. Acta*
635 **1390**, 339–345.

636 Peckmann, J., Thiel, V., Michaelis, W., Clari, P., Gaillard, C., Martire, L., Reitner, J.
637 (1999) Cold seep deposits of Beauvoisin (Oxfordian; southeastern France) and
638 Marmorito (Miocene; northern Italy): microbially induced authigenic carbonates. *Int.*

639 *J. Earth Sci.* **88**, 60–75.

640 Pearson, A., Seewald, J.S., Eglinton, T.I. (2005) Bacterial incorporation of relict carbon
641 in the hydrothermal environment of Guaymas Basin. *Geochim. Cosmochim. Acta* **69**,
642 5477–5486.

643 Pearson, A., Ingalls, A.E. (2013) Assessing the use of Archaeal lipids as marine
644 environmental proxies. *Annu. Rev. Earth Planet. Sci.* **41**, 359–384.

645 Pease, T.K., Van Vleet, E.S., Barre, J.S., Dickins, H.D. (1998) Degradation of glyceryl
646 ethers by hydrous and flash pyrolysis. *Org. Geochem.* **29**, 979–988.

647 Peters, K. E., Walters, C. C., Moldowan, J. M. (2004) The biomarker guide, 2nd edn.
648 Cambridge, UK: Cambridge University Press.

649 Rontani J.-F., Volkman J.K. (2003) Phytol degradation products as biogeochemical
650 tracers in aquatic environments. *Org. Geochem.* **34**, 1–35.

651 Rowland, S.J. (1990) Production of acyclic isoprenoid hydrocarbons by laboratory
652 maturation of methanogenic bacteria. *Org. Geochem.* **15**, 9–16.

653 Sandy, M. R., Lazăr, I., Peckmann, J., Birgel, D., Stoica, M., Roban, R. D. (2012)
654 Methane-seep brachiopod fauna within turbidites of the Sinaia Formation, Eastern
655 Carpathian Mountains, Romania. *Palaeogeogr. Palaeoclimatol. Palaeoecol.* **323-325**,
656 42-59.

657 Saito H., Suzuki N. (2010) Distribution of acyclic and cyclic biphytanediols in recent
658 marine sediments from IODP Site C0001, Nankai Trough. *Org. Geochem.* **41**, 1001–
659 1004.

660 Schouten S., Hoefs M.J., Koopmans M.P., Bosch H.-J., Sinninghe Damsté J.S. (1998)
661 Structural characterization, occurrence and fate of archaeal ether-bound acyclic and
662 cyclic biphytanes and corresponding diols in sediments. *Org. Geochem.* **29**, 1305–
663 1319.

664 Schouten, S., Wakeham, S. G., Hopmans, E. C., Sinninghe Damsté, J. S. (2003)
665 Biogeochemical evidence that thermophilic archaea mediate the anaerobic oxidation
666 of methane. *Appl. Environ. Microbiol.* **69**, 1680-1686.

667 Schouten, S., Baas, M., Hopmans, E.C., Sinninghe Damsté, J.S. (2008a) An unusual
668 isoprenoid tetraether lipid in marine and lacustrine sediments. *Org. Geochem.* **39**,
669 1033–1038.

670 Schouten, S., Baas, M., Hopmans, E.C., Reysenbach, A.-L., Sinninghe Damsté, J.S.
671 (2008b) Tetraether membrane lipids of Candidatus ‘‘*Aciduliprofundum boonei*’’, a
672 cultivated obligate thermoacidophilic euryarchaeote from deep-sea hydrothermal
673 vents. *Extremophiles* **12**, 119–124.

674 Schouten, S., Hopmans, E.C., Sinninghe Damsté, J.S. (2013) The organic geochemistry
675 of glycerol dialkyl glycerol tetraether lipids: A review. *Org. Geochem.* **54**, 19–61.

676 Stickland J.D.H., Parsons T.R.A. (1972) A Practical Handbook of Seawater Analysis.,
677 Fisheries Research Board of Canada, Ottawa.

678 Sturt H. F., Summons R. E., Smith K., Elvert M., Hinrichs K.-U. (2004) Intact polar
679 membrane lipids in prokaryotes and sediments deciphered by high-performance
680 liquid chromatography/electrospray ionization multistage mass spectrometry - new
681 biomarkers for biogeochemistry and microbial ecology. *Rapid Commun. Mass*
682 *Spectrom.* **18**, 617–628.

683 Sutton, P.A., Rowland, S.J. (2012) High temperature gas chromatography–time-of-flight-
684 mass spectrometry (HTGC–ToF-MS) for high-boiling compounds. *J. Chromatogr.*
685 *A.* **1243**, 69–80.

686 Sutton, P.A., Rowland, S.J. (2014) Determination of the content of C_{80} tetraacids in
687 petroleum. *Energy Fuels* **28**, 5657–5669.

688 Teske, A., Callaghan, A.V., LaRowe, D.E. (2014) Biosphere frontiers of subsurface life
689 in the sedimented hydrothermal system of Guaymas Basin. *Front. Microbiol.* **5**,
690 doi:10.3389/fmicb.2014.00362

691 Thiel, V., Peckmann, J., Seifert, R., Wehrung, P., Reitner, J., Michaelis, W. (1999)
692 Highly isotopically depleted isoprenoids: molecular markers for ancient methane
693 venting. *Geochim. Cosmochim. Acta* **63**, 3959–3966.

694 Weijers, J.W.H., Schouten, S., Hopmans, E.C., Geenevasen, J.A.J., David, O.R.P.,
695 Coleman, J.M., Pancost, R.D., Sinninghe Damsté, J.S. (2006) Membrane lipids of
696 mesophilic anaerobic bacteria thriving in peats have typical archaeal traits. *Environ.*
697 *Microbiol.* **8**, 648–657.

698 Weijers, J.W.H., Schouten, S., van den Donker, J.C., Hopmans, E.C., Sinninghe Damsté,
699 J.S. (2007) Environmental controls on bacterial tetraether membrane lipid
700 distribution in soils. *Geochim. Cosmochim. Acta* 71, 703–713.

701 Wuchter, C., Schouten, S., Wakeham, S.G., Sinninghe Damsté, J.S. (2005) Temporal and
702 spatial variation in tetraether membrane lipids of marine Crenarchaeota in
703 particulate organic matter: Implications for TEX_{86} paleothermometry.
704 *Paleoceanography* **20**, doi:10.1029/2004PA001110

705 Xie, S., Lipp, J.S., Wegener, G., Ferdelman, T.G., Hinrichs, K.-U. (2013) Turnover of
706 microbial lipids in the deep biosphere and growth of benthic archaeal populations.
707 *Proc. Natl. Acad. Sci. USA* **110**, 6010-6014.

708 Yang H., Pancost R.D., Tang C., Ding W., Dang X., Xie S. (2014) Distributions of
709 isoprenoid and branched glycerol dialkanol diethers in Chinese surface soils and a
710 loess–paleosol sequence: Implications for the degradation of tetraether lipids. *Org.*
711 *Geochem.* **66**, 70–79.

712 Yoshinaga, M.Y., Lazar, C.S., Elvert, M., Lin, Y-S., Zhu, C., Heuer, V.B., Teske, A.,
713 Hinrichs, K.-U. (2015) Possible roles of uncultured archaea in carbon cycling in
714 methane-seep sediments. *Geochim. Cosmochim. Acta*, **164**, 35-52.

715 Zhu, R., Evans, T.W., Wörmer, L., Lin, Y.-S., Zhu, C., Hinrichs, K.-U. (2013a) Improved
716 sensitivity of sedimentary phospholipid analysis resulting from a novel extract
717 cleanup strategy. *Org. Geochem.* **65**, 46–52.

718 Zhu C., Lipp J.S., Wörmer L., Becker K.W., Schröder J., Hinrichs K.-U. (2013b)
719 Comprehensive glycerol ether lipid fingerprints through a novel reversed phase liquid
720 chromatography–mass spectrometry protocol. *Org. Geochem.* **65**, 53–62.

721

722

723

724

Compounds	Abbreviation	Structural illustration	Distribution				
			Leg201-1227	Marmorito seep carbonate	Guaymas Basin 4568	Hot spring T-15	*N. maritimus* late stat. phase
glycerol dialkyl glycerol tetraether	GDGT	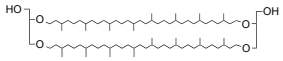	+	+	+	+	+
glycerol dialkyl glycerol triether alcohol	GDGTol	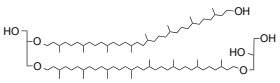	+	+	+	n.d.	+
glycerol dialkyl glycerol triether acid	GDGTA	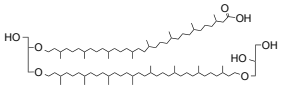	+	+	n.d.	n.d.	n.d.
glycerol dibiphytanol diether	GDD	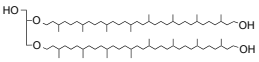	+	+	+	+	+
glycerol dibiphytanol diether monoacid	GDDA	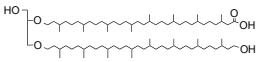	+	+	+	n.d.	+
glycerol dibiphytanol diether diacid	GDDAA	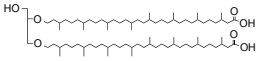	n.d.	+	n.d.	n.d.	n.d.
glycerol monobiphytanyl glycerol diether	GMGD	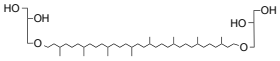	+	+	+	n.d.	n.d.
glycerol monobiphytanol monoether	GMM	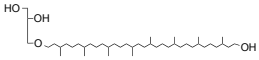	+	+	+	n.d.	n.d.
glycerol monobiphytanol monoether acid	GMMA	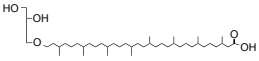	n.d.	+	n.d.	n.d.	n.d.
biphytanic diol	bpdiol	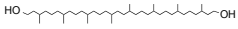	+	+	+	+	+
biphytanic monoacid	bpmonoacid/ol	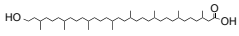	+	+	n.d.	n.d.	n.d.
biphytanic diacid	bpdiacid	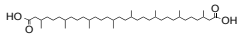	n.d.	+	n.d.	n.d.	n.d.
H-shaped glycerol monoalkyl glycerol tetraether	H-GMGT	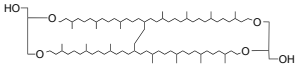	+	+	+	+	n.d.
H-shaped glycerol monoalkyl diether	H-GMD	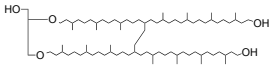	+	+	+	+	n.d.
H-shaped C_{80} tetrol	H-tetrol	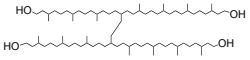	+	+	+	+	n.d.
H-shaped C_{80} monoacid	H-monoacid	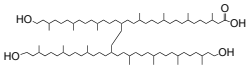	n.d.	n.d.	+	n.d.	n.d.
H-shaped C_{80} diacid	H-diacid	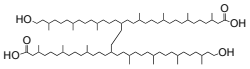	n.d.	n.d.	+	n.d.	n.d.
H-shaped C_{80} triacid	H-triacid	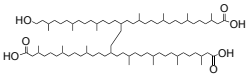	n.d.	n.d.	+	n.d.	n.d.
H-shaped C_{80} tetraacid	H-tetraacid	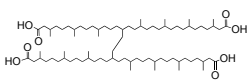	n.d.	n.d.	+	n.d.	n.d.

725

726 **Table 1.** Compound classes discussed in the paper. Illustrated structures show only the
727 acyclic biphytane derivatives. Constitutional isomers are not included. Representative
728 samples showing the distribution of GDGT and degradation products in various
729 environment settings and cell. '+' compound detected, 'n.d.' compound not detected.

730

731

732

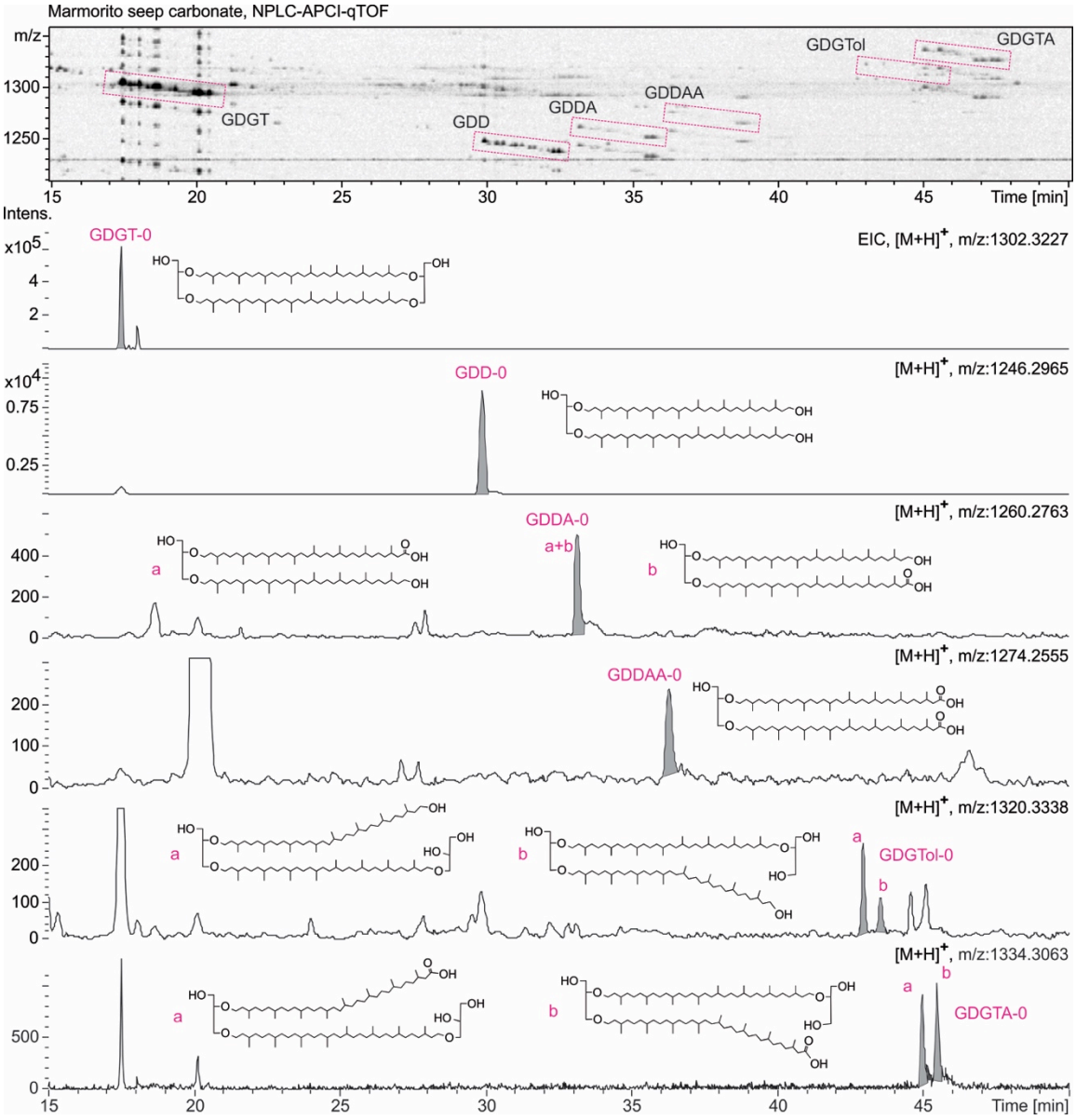

Fig. 1a

Density maps and extracted ion chromatograms (EICs) of NPLC-APCI-qTOF showing the detection of isoprenoidal GDGT-0 and its hydroxylated and carboxylated derivatives with two (Fig. 1a) or one biphytane units (Fig. 1b) in the Marmorito seep carbonate. Multiple isomers were observed for GDDA, GDGTol, GDGTA, GMM and GMGD and are labeled as ‘a’ and ‘b’. The isomeric composition of GMGD, ‘a’ and ‘b’, may provide insights regarding the regioisomerism of GDGTs and will be subject of a future report.

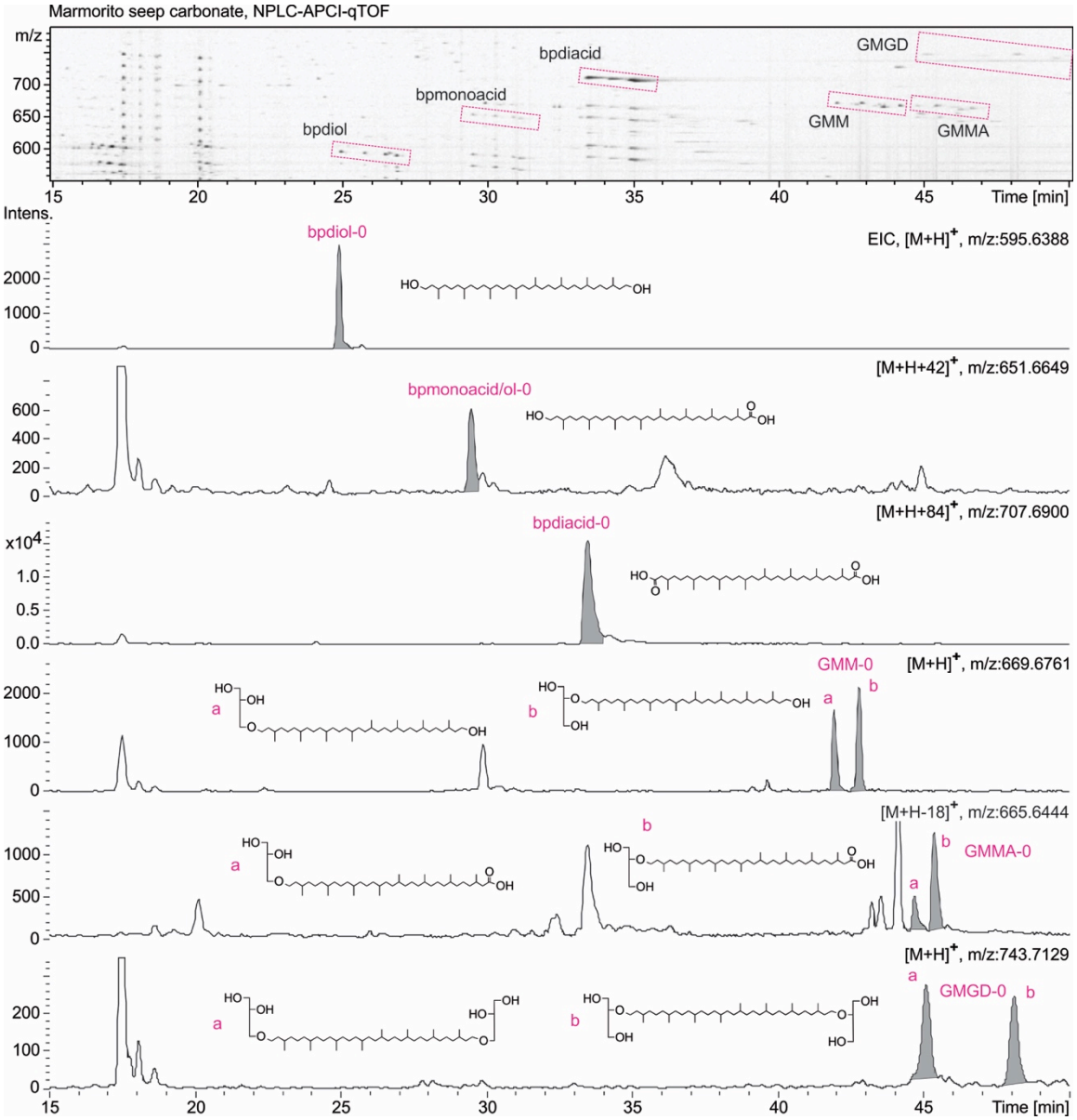

Fig. 1b

Density maps and EICs of NPLC-APCI-qTOF showing the detection of isoprenoidal GDGT-0 and hydroxylated and carboxylated derivatives with two (Fig. 1a) or one, biphytane units (Fig. 1b) in the Marmorito seep carbonate. Multiple isomers were observed for GDDA, GDGTol, GDGTA, GMM and GMGD and are labeled as 'a' and 'b'. The isomeric composition of GMGD, 'a' and 'b', may provide insights regarding the regioisomerism of GDGTs.

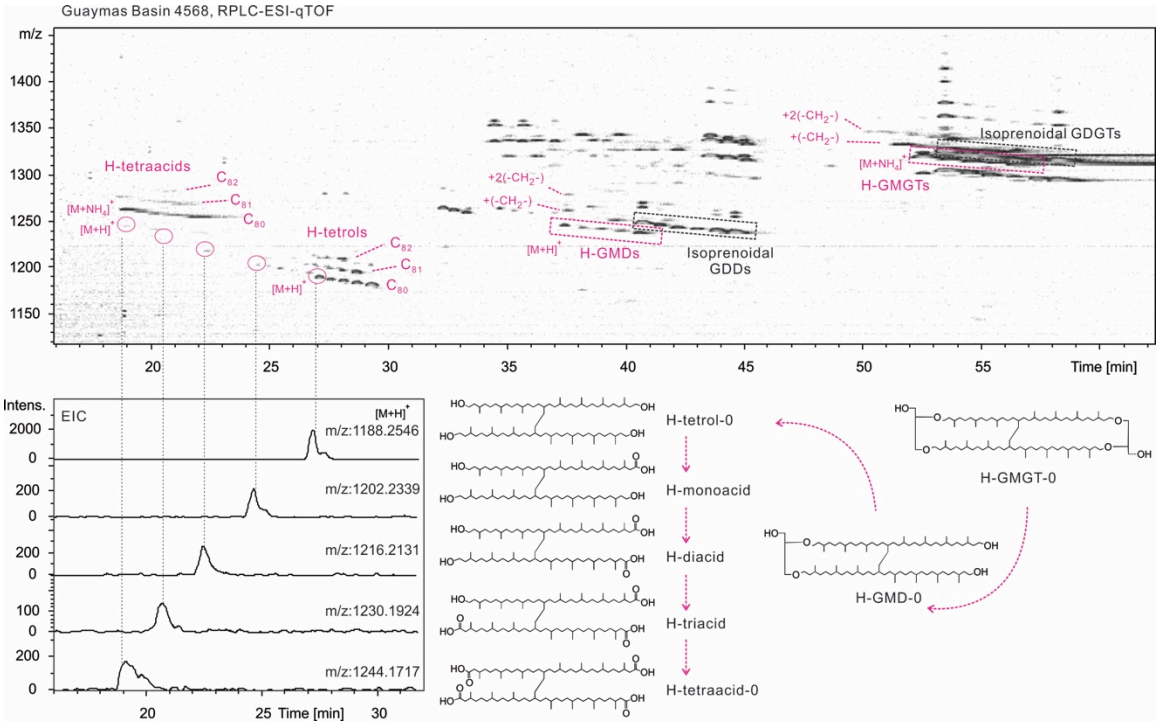

Fig. 2 Density maps and EICs derived from RPLC-ESI-qTOF analysis showing the detection of H-GMGTs and their hydroxylated and carboxylated derivatives in a hydrothermal sediment from the Guaymas Basin. Stepwise oxidation of the four hydroxyl groups in the H-tetrols possibly generated C_{80} mono-, di-, tri- and H-tetraacids. Mono- and di-methylated H-GMGTs, H-GMDs and corresponding C_{81}, C_{82} H-tetrols and H-tetraacids were also detected. Molecular structures of the intermediates are suggested. Isomers of monoacid, diacid and triacid may exist but could not be separated with the present LC methods.

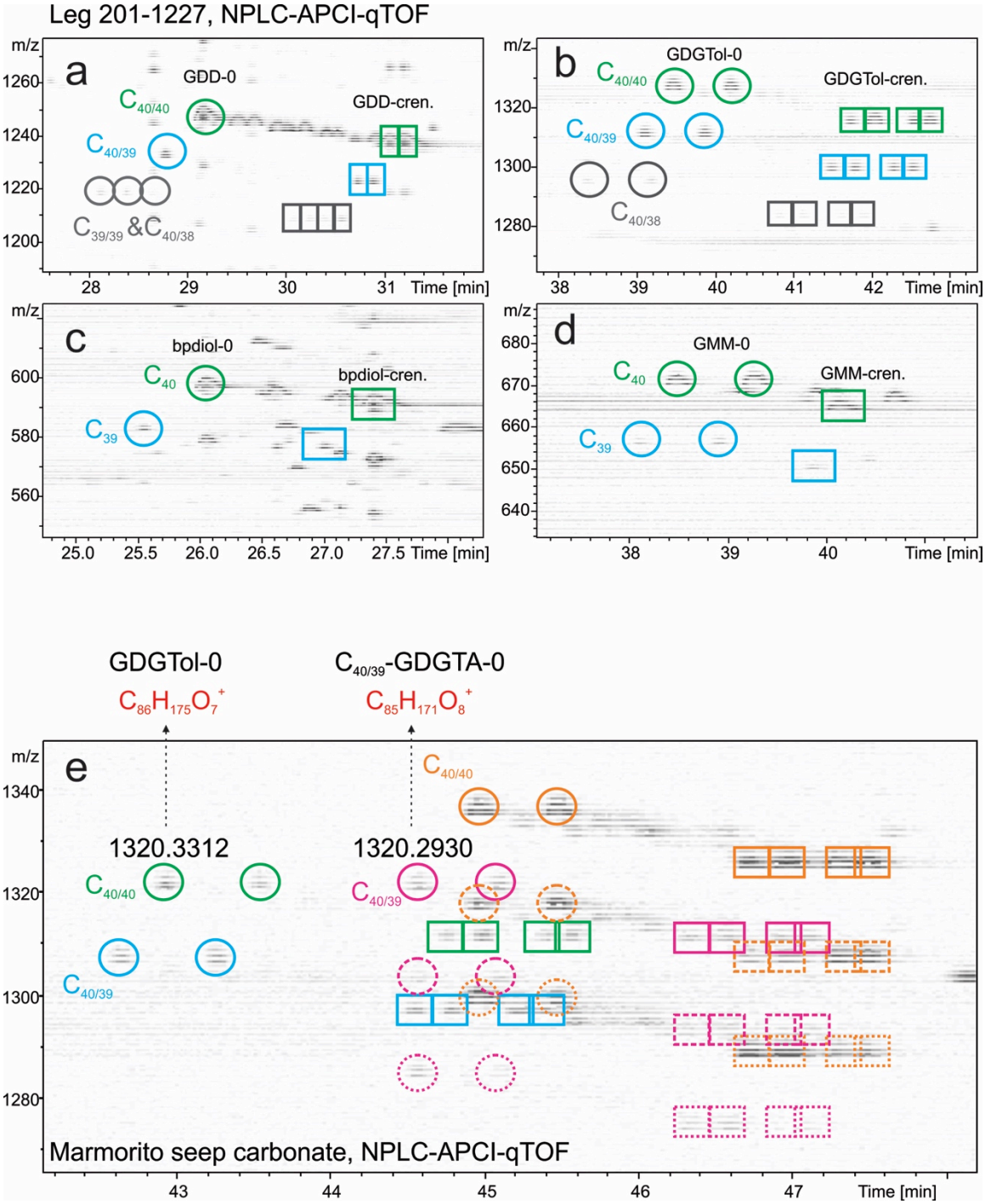

765

766 Fig. 3 Density maps of NPLC-APCI-qTOF showing in one marine sediment (Leg 201-
767 1227) the detection of GDD, GDGTol, biphytane diol, GMM and their co-occurring
768 further degradation derivatives with C_{39} and C_{38} based isoprenoids, (a-d). Highlighted are
769 the most dominant components including the GDGT-0 (open circle) and crenarchaeol-
770 related (rectangle) compounds. Different compound classes are also color coded. C_{40}

771 hydroxyl derivatives are in green, C_{39} in blue and the C_{38} related in grey, C_{40} carboxyl
772 derivatives are in orange and C_{39} in pink. Multiple isomers occur due to different ether
773 bonding and ring arrangements. The occurrence of $C_{40/39}$-GDGTA was shown in one
774 sample of Marmorito seep carbonate (e). The molecular ion of $C_{40/39}$-GDGTA-0 and
775 GDGTol-0 gives similar but distinguishable masses, m/z: 1320.2930 and 1320.3312,
776 respectively. Under APCI, dehydrated ions of carboxyl derivatives occurred (highlighted
777 ions with dashed lines).

778

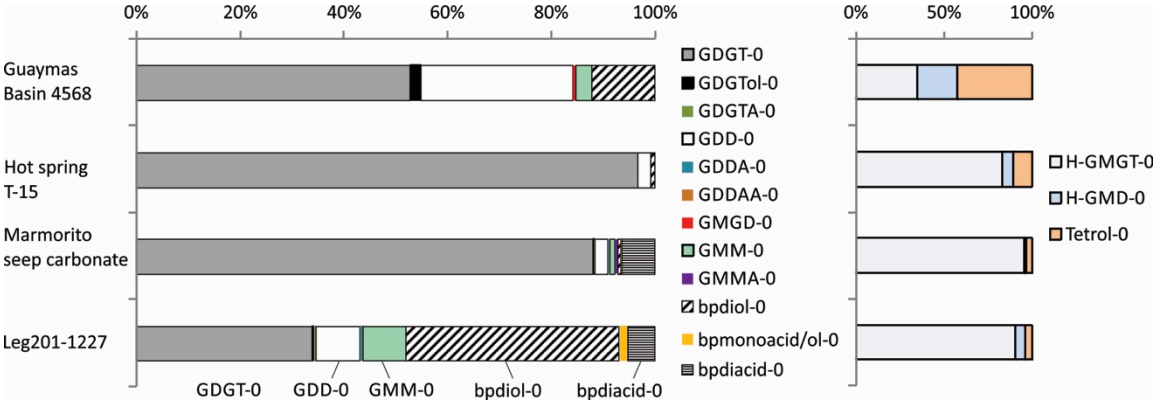

Fig. 4 Relative abundances of diagenetic derivatives of GDGT-0 (left panel) and H-GMGT-0 (right panel) in four representative environmental samples.

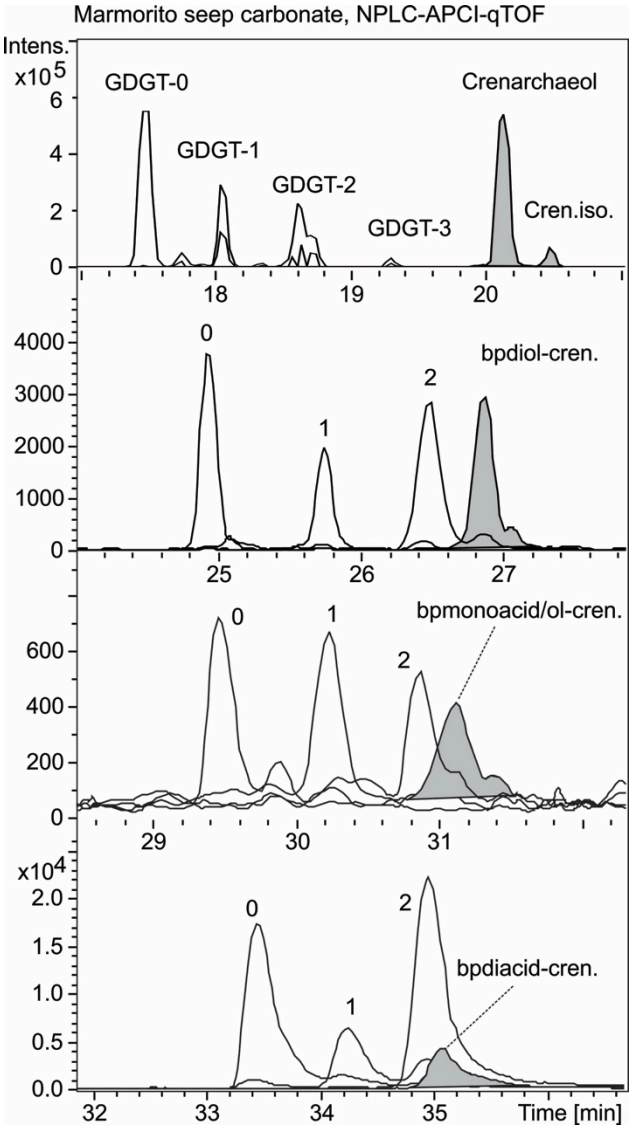

788

789 Fig. 5 Extracted ion chromatograms from NPLC-APCI-qTOF analysis, showing the
790 distribution of GDGT, bpdiol, bpmonoacid/ol and bpdiacids in a seep carbonate,
791 Marmorito. Peaks of crenarchaeol and its related derivatives are shaded; crenarchaeol
792 derivatives have decreased abundances in the acid fractions.

793

794

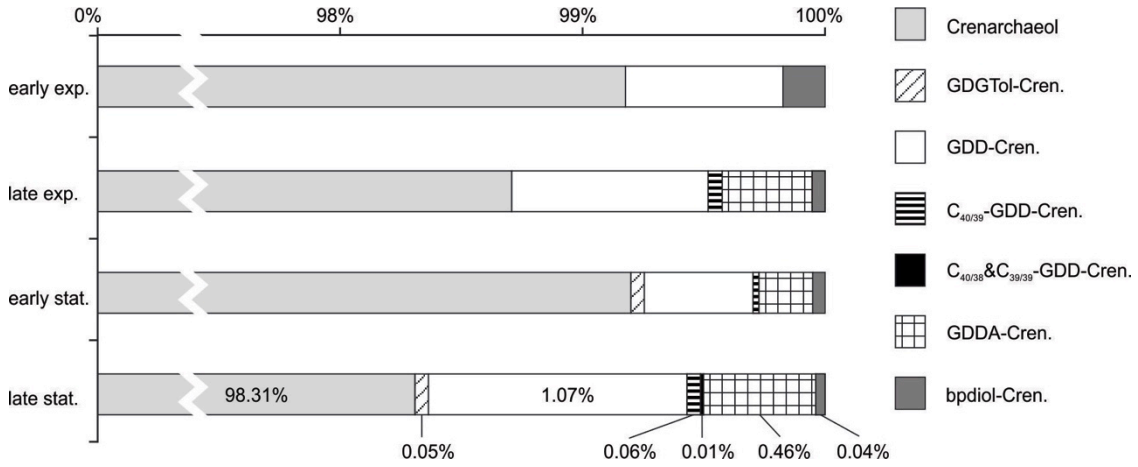

795

796

797

798 Fig. 6 The relative abundance of core crenarchaeol and its related hydroxyl, carboxyl and

799 C_{39} and C_{38} based derivatives in different growth phases of *N. maritimus*.

800

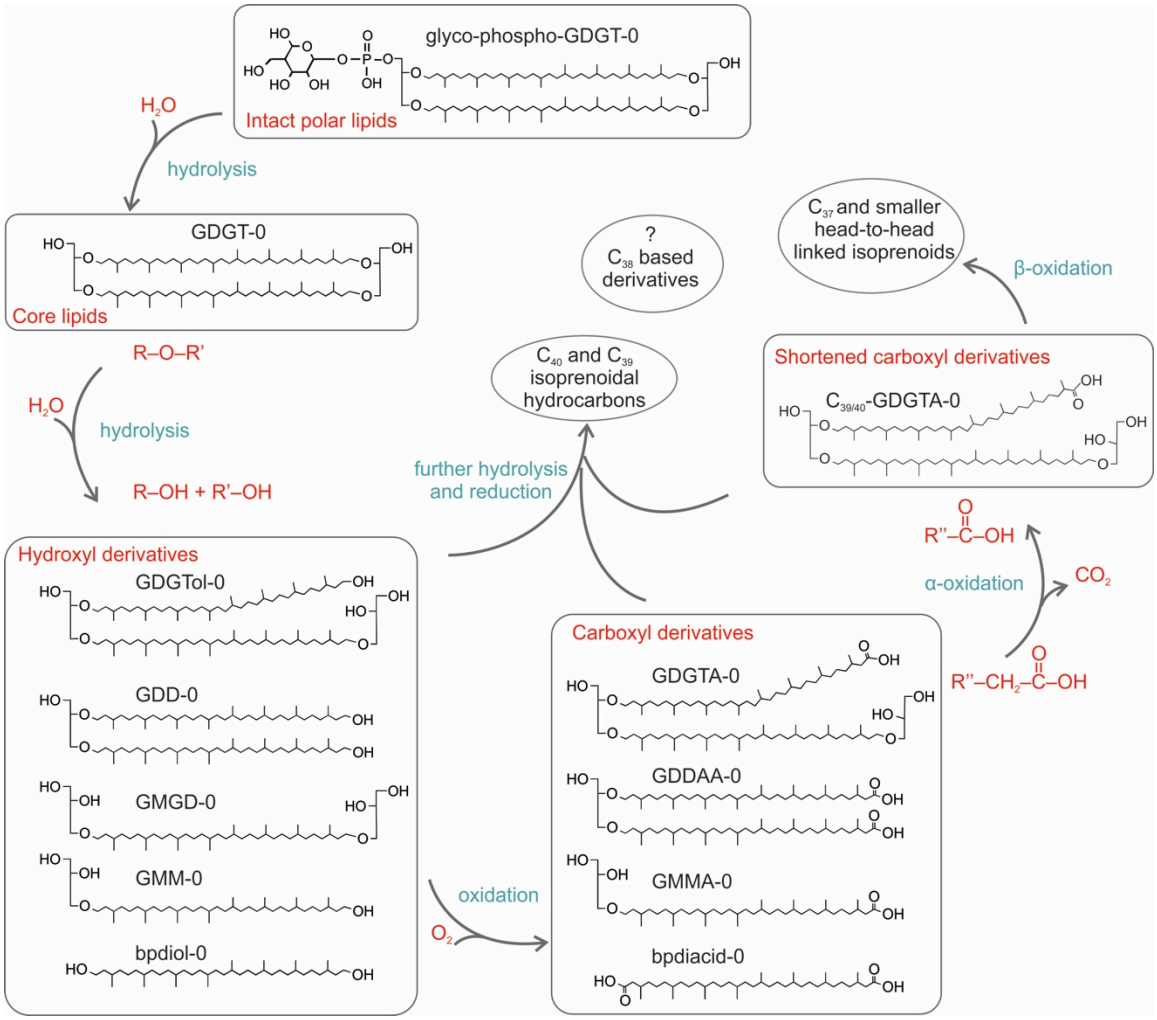

Fig. 7 Hypothetical scheme showing the suggested diagenetic pathways of GDGTs. GDGT-0 and its related IPL and degradation derivatives are used as an example. In the flow chart, R, R' and R'' represent different alkyl chains. Intermediate components, such as GDDA, bpmonoacid/ol are not included. The formation of C_{38} based isoprenoids is not clear and thus is labeled with '?'.

Supplementary information

Sample preparation

1. **Hot spring sediment T-15**

Sediment was collected from the bottom of a geothermal wells located in Ruidian (Jinze hot spring: N 25.44138°, E98.46004°, Elevation:1740m. Tengchong County, Yunnan Province, China), with the water pH of 6.71 and temperature of 80.6 °C. Roughly 5 g of freeze-dried sediment was extracted in an ultrasonic bath with methanol (MeOH; twice), methanol-dichloromethane (DCM; 1:1, v/v; twice) and finally DCM (twice). All supernatants were collected in a flask and completely dried under N_2. The total lipid extract was fractionated over a pre-activated silica gel chromatography into apolar (alkane) and polar (intact polar GDGTs and GDGT core lipids) fractions using *n*-hexane-DCM (9:1, v/v) and DCM-MeOH (1:1, v/v) as eluents respectively. The polar fraction was used for the lipid analysis in this study.

2. H-tetrol standards

An oilfield calcium naphthenate deposit was Soxhlet extracted sequentially (dichloromethane/*n*-hexane, 1/1, v/v, 300 mL, 8h; toluene/acetone, 3/2, v/v, 250 mL, 6h; propan-2-ol/dichloromethane, 4/1, v/v, 250mL, 6h) to remove interstitial oil and the residue dried (overnight, 70˚C) before acidification by heating (70˚C, overnight) in a capped and sealed vial with hydrochloric acid (3 mL) and cyclohexane (3 mL). The acidified organic fraction was recovered by extraction into diethylether (DEE; 3 x 5 mL) by mixing (vortex 10 s) and centrifugation (2500 rpm/3 min). Solvent was removed from

834 the decanted supernatant under blow-down (N_2, 70˚C) prior to dilution in DEE/0.1%
835 ammonia (8 mL), loading on a pre-conditioned (1% aqueous ammonia, 20 mL; water, 20
836 mL; DEE, 10 mL) SAX solid phase extraction cartridge (Sigma-Aldrich Company Ltd.,
837 Dorset, UK; DSC-SAX, 12 mL, 2 g) and sequentially eluting the cartridge with 20 mL
838 volumes of DEE, dichloromethane and DEE/2% formic acid (FA). Solvent was removed
839 from the DEE/2% FA fraction ('acid fraction') under blow-down (N_2, 70˚C) and an
840 aliquot per-trimethylsilylated with BSTFA/1% TMCS (Sigma-Aldrich Company Ltd.,
841 UK; ca. 50 µL, 70˚C, 1 hr) before dilution in cyclohexane for analysis using high
842 temperature gas chromatography (HTGC; Fig. SX1), or per-methylation for infusion
843 electrospray ionization/mass spectrometry (ESI/MS; Fig. SX2). An aliquot of the isolated
844 acid fraction was diluted in DEE for infrared spectroscopy (Fig. SX3).
845
846 The isolated acid fraction was reduced to alcohols by treatment with lithium aluminum
847 hydride (LithAl; Sigma-Aldrich Company Ltd., UK; 1M in DEE). Dried acid fraction
848 was dissolved in a small volume (ca. 1 mL) dry DEE (sodium wire) and transferred with
849 washings to a small three-neck flask with Teflon flea and fitted with a Subaseal, calcium
850 chloride drying tube condenser and a glass stopper, all over a magnetic stirring block.
851 LithAl solution (ca. 3 mL) was pumped into the flask under nitrogen through the
852 Subaseal whilst stirring, additional dry DEE (ca. 5mL) was added through the condenser
853 to break up formed solids, before placing a bowl of warm water under the flask for 10
854 minutes. After the reaction vessel had cooled, wet DEE (prepared by mixing DEE and
855 water in separating funnel and drawing off aqueous phase) was added (10 mL, drop-wise
856 at first) to hydrolyse unreacted hydrides, followed by drop-wise addition of sulphuric

857 acid (10% aqueous; ca. 1 mL) to destroy remaining LithAl. The contents of the flask
858 were transferred with washings (ca. 3 mL, 10% $H_2SO_{4(aq)}$) to a separating funnel and the
859 organic phase ('alcohol fraction') collected after washing with water (3 x 3 mL). Solvent
860 was removed from the alcohol fraction by blow-down (N_2, 70˚C) and aliquots prepared
861 for HTGC, ESI/MS and IR spectroscopy as above. All solvents were HPLC grade
862 (Rathburn Chemicals Ltd., Walkerburn, UK or Fisher Scientific UK Ltd., Loughborough,
863 UK) or LC/MS grade (Chromasolv®; Sigma-Aldrich Company Ltd., Dorset, UK), water
864 was Elga Maxima (18.2 mΩ; Elga Ltd., Buckinghamshire, UK).
865
866 Reduction of the tetraacids to tetrols was monitored using HTGC (Fig. SX1), ESI/MS
867 (Fig. SX4 and SX5) and IR spectroscopy (Fig. SX3). The HTGC system comprised an
868 Agilent 6890 GC fitted with cool-on-column inlet (+3˚C track oven mode; 0.5 µL manual
869 injection), flame ionization detector (435˚C) and Varian VF-5ht Ultimetal column (15 m
870 x 0.25 mm x 0.1 µm) with helium carrier gas (1 ml min^{-1}, constant flow) and oven
871 programme from 40 – 430˚C at 10˚C min^{-1} with 10 min hold.
872
873 Infusion ESI/MS was carried out in positive ionization mode using a Finnigan Mat
874 LCQ™ (ThermoFinnigan, San Jose, CA, USA) with ESI interface. Samples were diluted
875 in propan-2-ol/10mM ammonium acetate and infused at 3 µL min^{-1} with a Hamilton
876 (Reno, CA, USA) 1725N (250 µL) syringe using the built-in syringe pump. Mass spectral
877 data were acquired (and averaged over 1 minute) and processed using Xcalibur software.
878 Typical instrument parameters were: source voltage (±) 4.5 kV; capillary voltage (±) 60
879 V; capillary temperature 200 °C; nitrogen sheath gas flow rate 24 (arbitrary units).

Instrumental parameters were optimised on the most abundant ion using the autotune function.

Infrared spectroscopy was carried out using a Bruker Alpha Platinum ATR (Bruker Optik GmbH, Ettlingen, Germany) by measuring 32 sample scans (resolution 4 cm^{-1}; transmittance) and recording data between 4000 – 375 cm^{-1}. Background comprised 32 scans without sample.

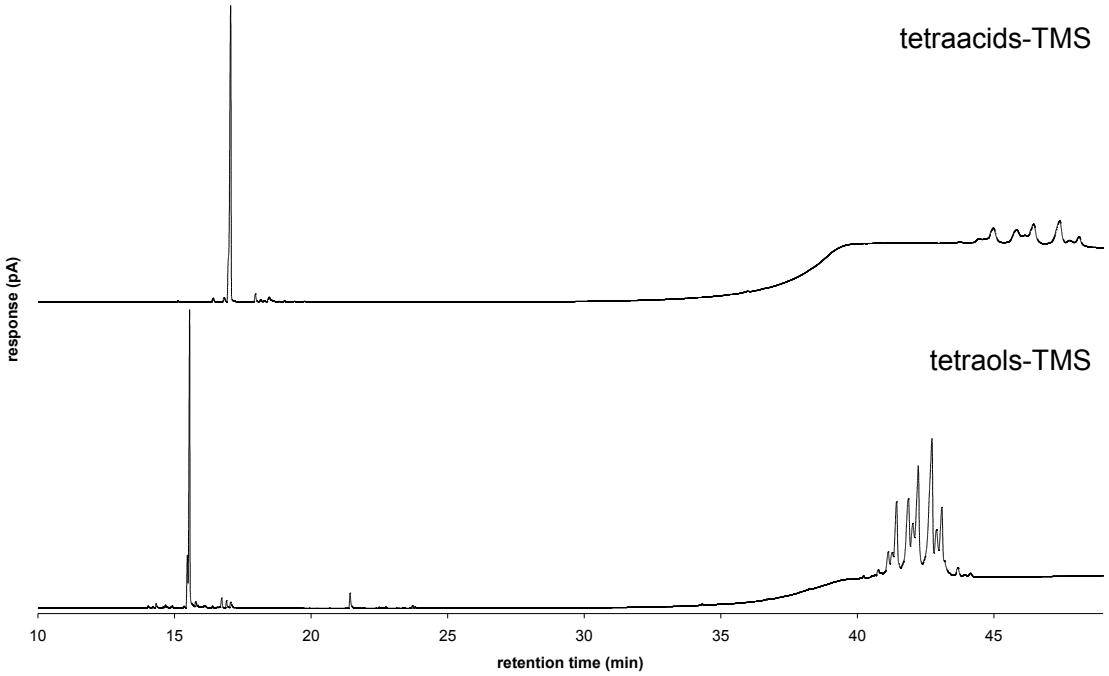

Figure SX1. High temperature gas chromatograms of trimethylsilylated tetraacids obtained from an oilfield deposit (upper) and lower the trimethylsilylated tetraols obtained following LithAl reduction (lower).

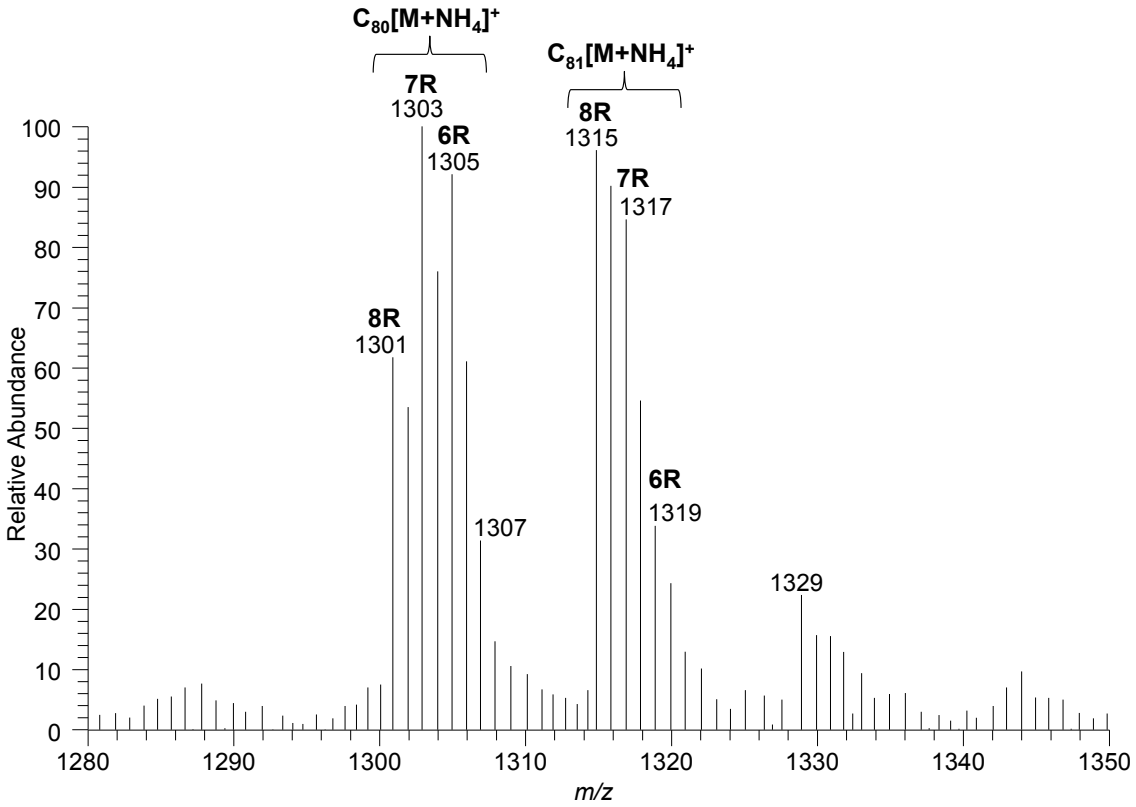

893

894 Figure SX2. Averaged mass spectrum from HPLC-electrospray ionization (+ve) mass

895 spectrometry of per-methylated esters of tetraacids obtained from an oilfield deposit (nR

896 refers to the number of cyclopentyl rings in the molecule)

897

898

899

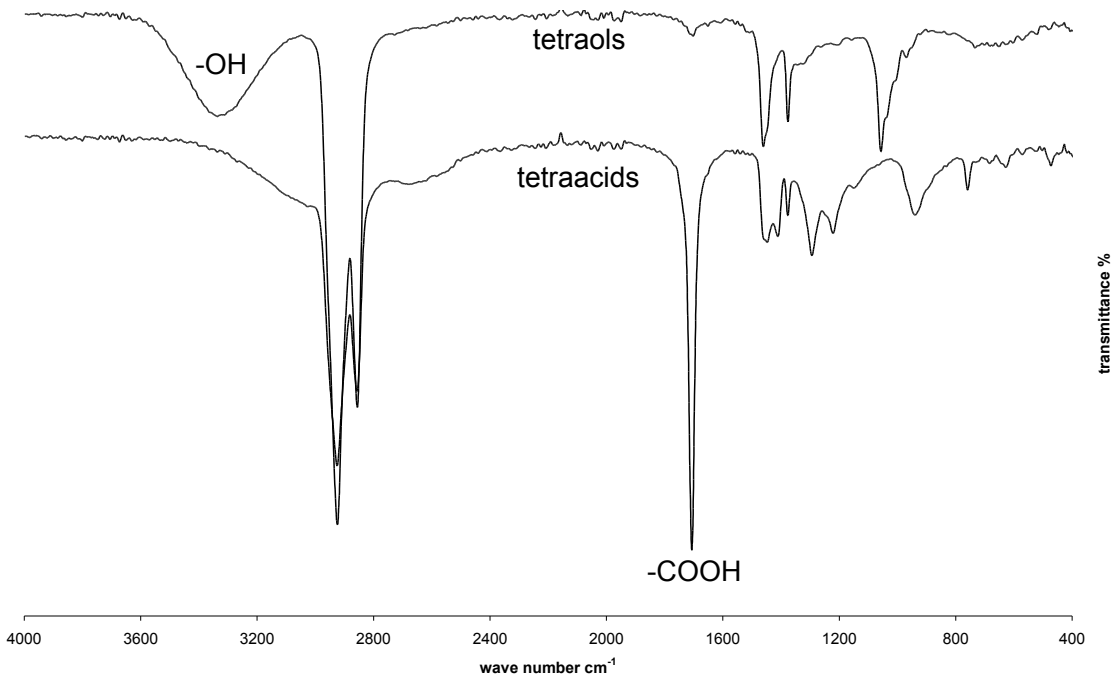

900

901 Figure SX3. FTIR transmittance spectra of tetraacids isolated from an oilfield deposit

902 (lower) and tetraols produced from the tetraacids by LithAl reduction (upper).

903

904

905

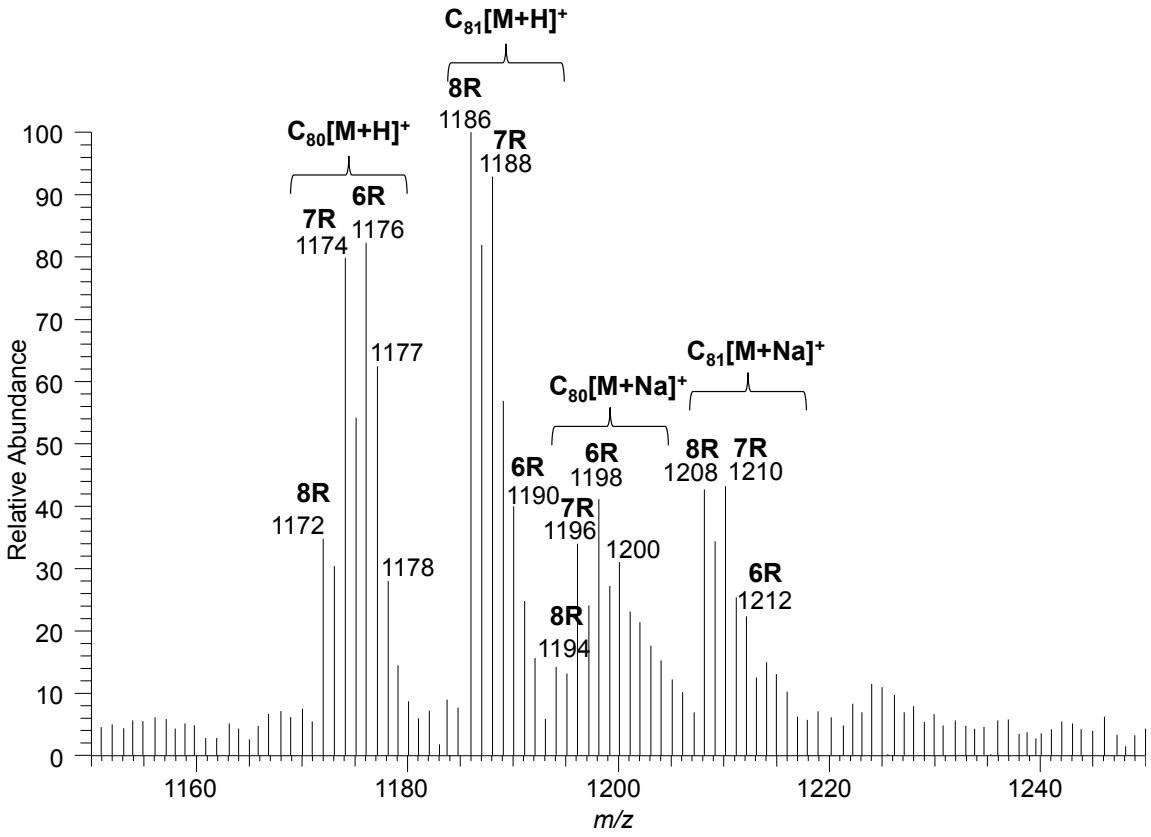

906

907 Figure SX4. Infusion electrospray ionization (+ve) mass spectrum of underivatised

908 tetraols obtained from the LithAl reduction of tetraacids from an oilfield deposit (nR

909 refers to the number of cyclopentyl rings in the molecule).

910

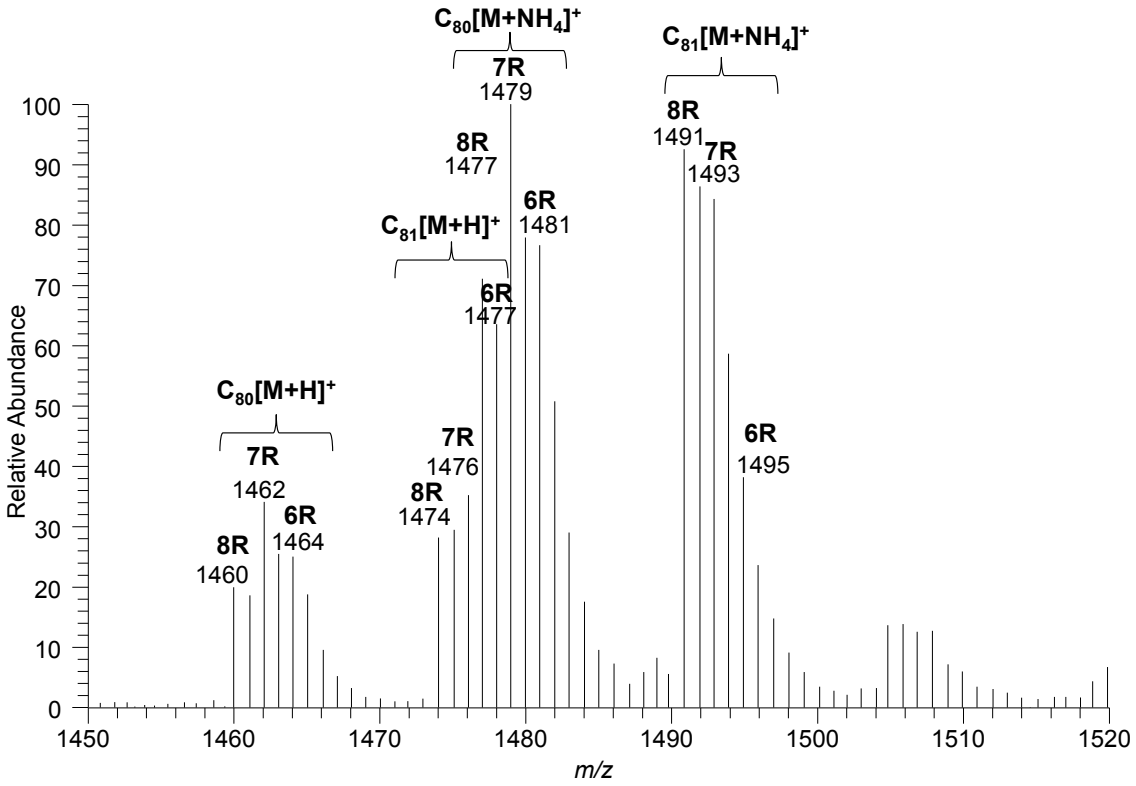

Figure SX5. Infusion electrospray ionization (+ve) mass spectrum of per-trimethylsilylated tetraols obtained from the LithAl reduction of tetraacids from an oilfield deposit (nR refers to the number of cyclopentyl rings in the molecule).

3. Acid hydrolysis of GDGT-0 standard

GDGT-0 standard was isolated with a semi-preparative LC protocol (as described in Zhu et al., 2014) from acid-hydrolyzed biomass of *Archaeoglobus fulgidus*. Strong acid hydrolysis was then performed with 10% methanolic HCl and GDGT-0 standard under 70 °C for 96 hours. After dried with a N_2 flow the treated sample was dissolved in *n*-hexane for LC-APCI-MS analysis.

924

925 **Reference:**

926 Zhu, C., Meador, T.B., Dummann, W., Hinrichs, K.-U., 2014. Identification of unusual
927 butanetriol dialkyl glycerol tetraether and pentanetriol dialkyl glycerol tetraether lipids in
928 marine sediments. *Rapid Commun. Mass Spectrom.* 28, 332–338.

929

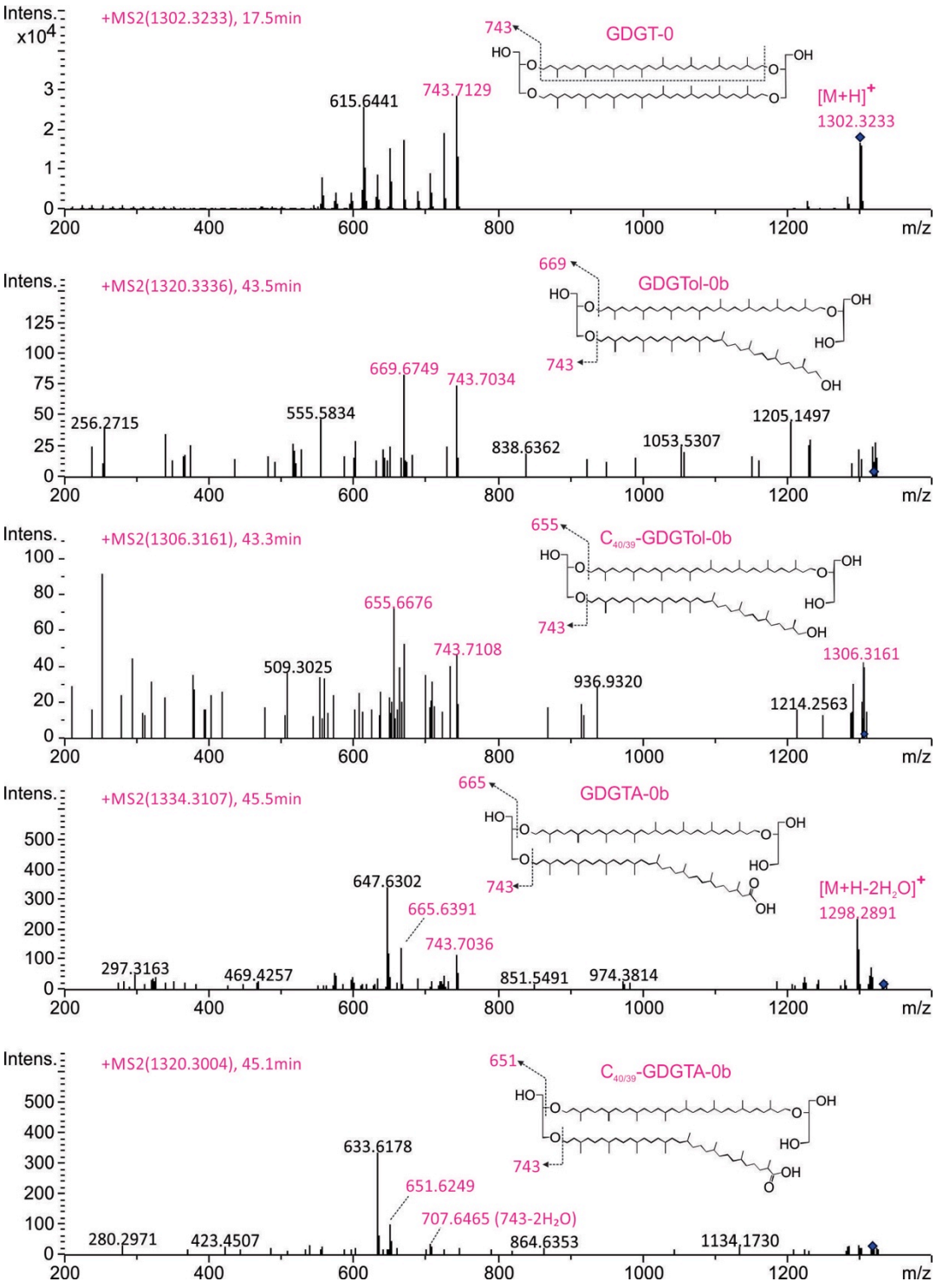

930

931

932 **Figure S1a.** MS^2 fragmentation patterns supporting the identification of GDGT-0,
933 GDGTol-0 and GDGTA-0 in Fig. 1a, and $C_{40/39}$-GDGTol-0 and $C_{40/39}$-GDGTA-0 in Fig.
934 3e.

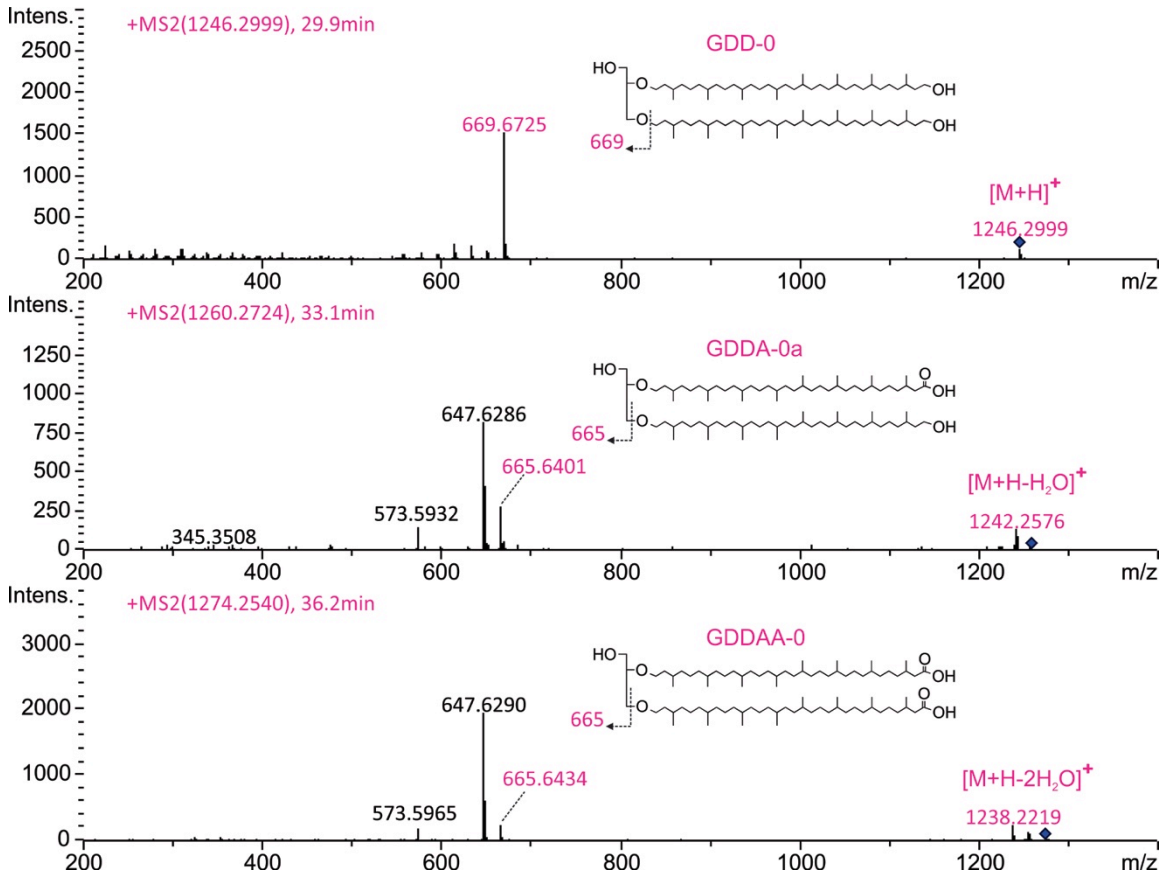

Figure S1b. MS^2 fragmentation patterns supporting the identification of GDD-0, GDDA-0 and GDDAA-0 in Fig. 1a**.**

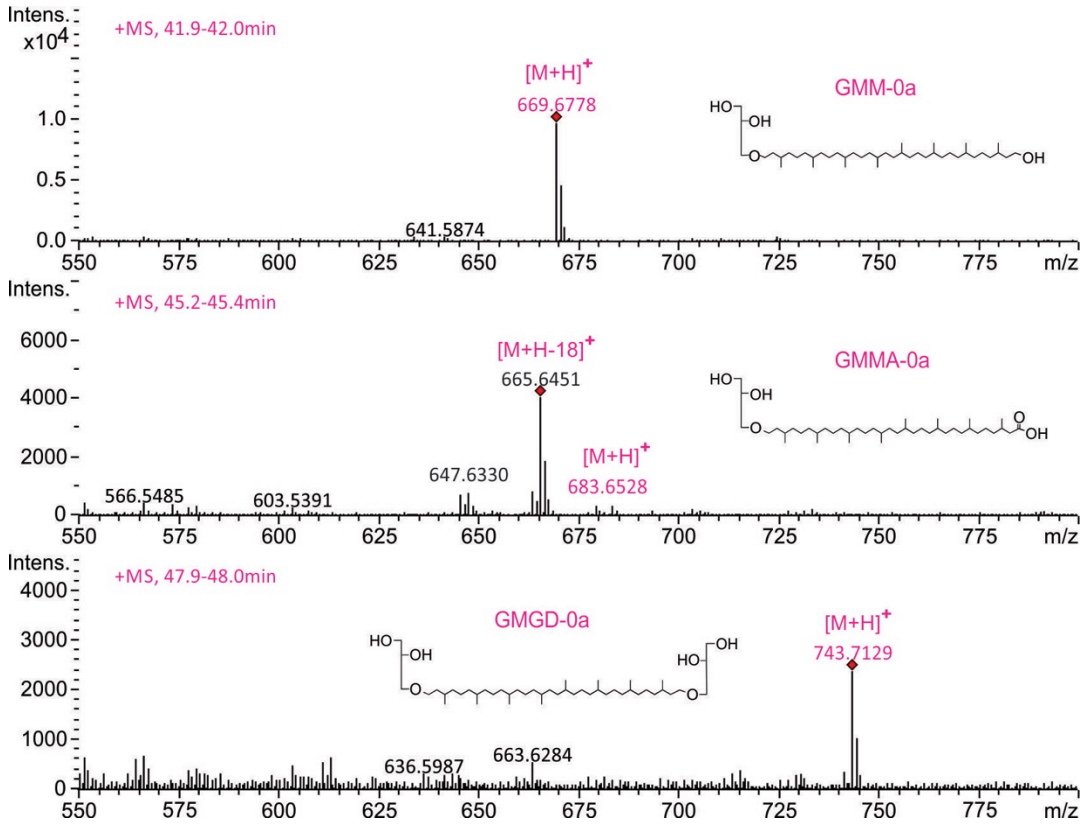

Figure S1c. MS[1] ions supporting the identification of GMM-0, GMMA-0 and GMGD-0 in Fig. 1b.

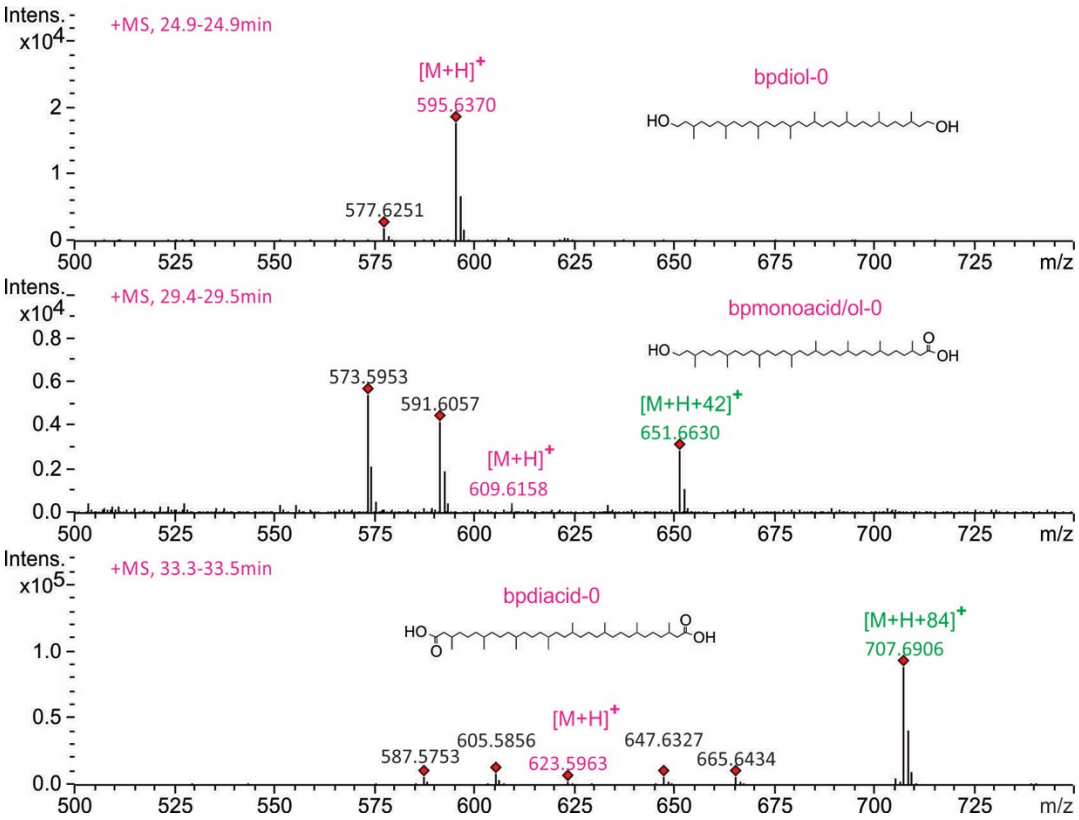

Figure S1d. MS^1 ions supporting the identification of bpdiol-0, bpmonoacid/ol-0 and bpdiacid-0 in Fig. 1b.

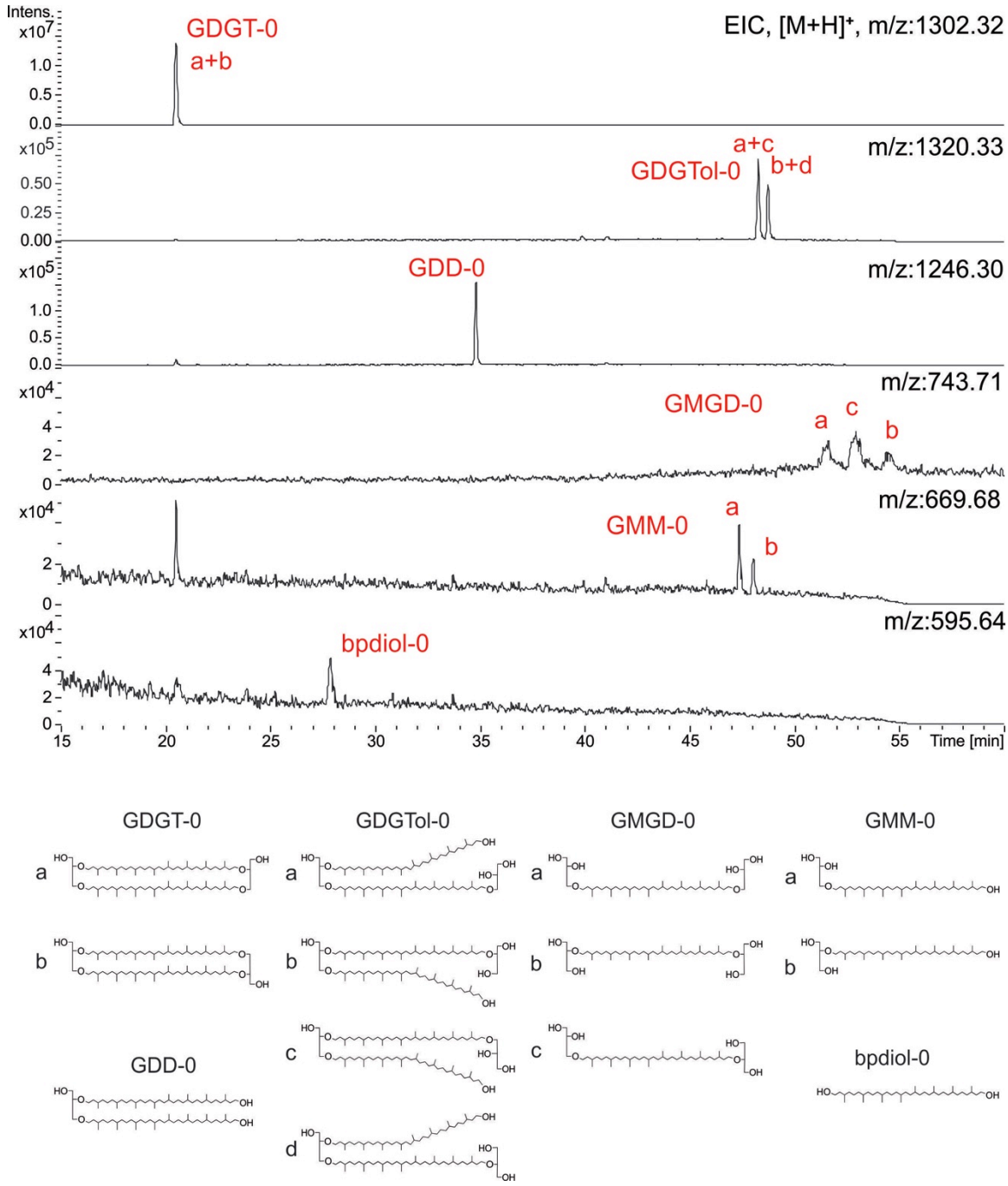

957

958

959 **Figure S2**

960 Major hydroxyl derivatives released from GDGT-0 by chemical degradation, a mild ether
961 cleavage conducted by adding 1000ng GDGT-0 into 1mL of 10% HCl in methanol, and

heated to 70 °C for 96 hours. The composition of GMGDs indicated a nearly 1:1 mixture of parallel and anti-parallel GDGT-0.

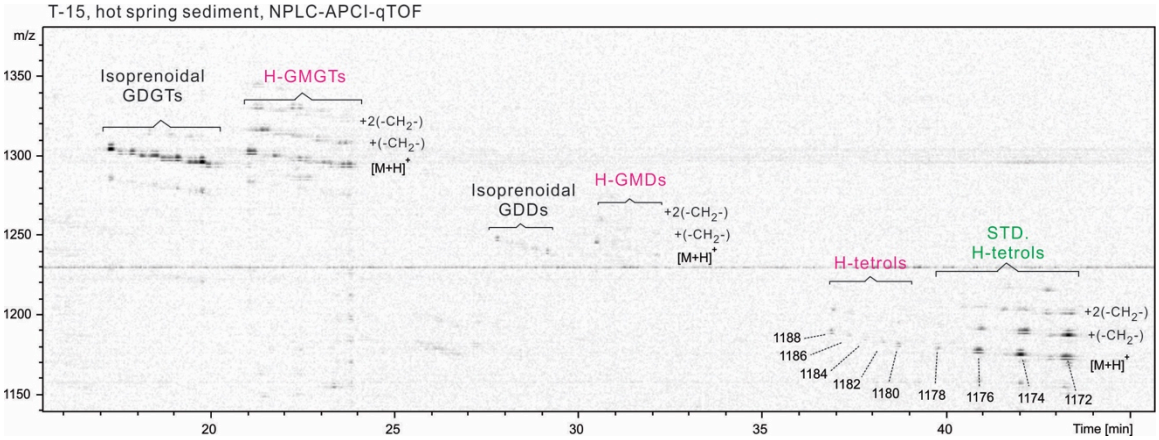

Figure S3

Density maps of NPLC-APCI-qTOF showing the occurrence of H- GDGTs and their degradation derivatives in the hot spring sediment, T-15. The identification of H-tetrols are confirmed by their similar chromatographic behavior with added standards (green color text).

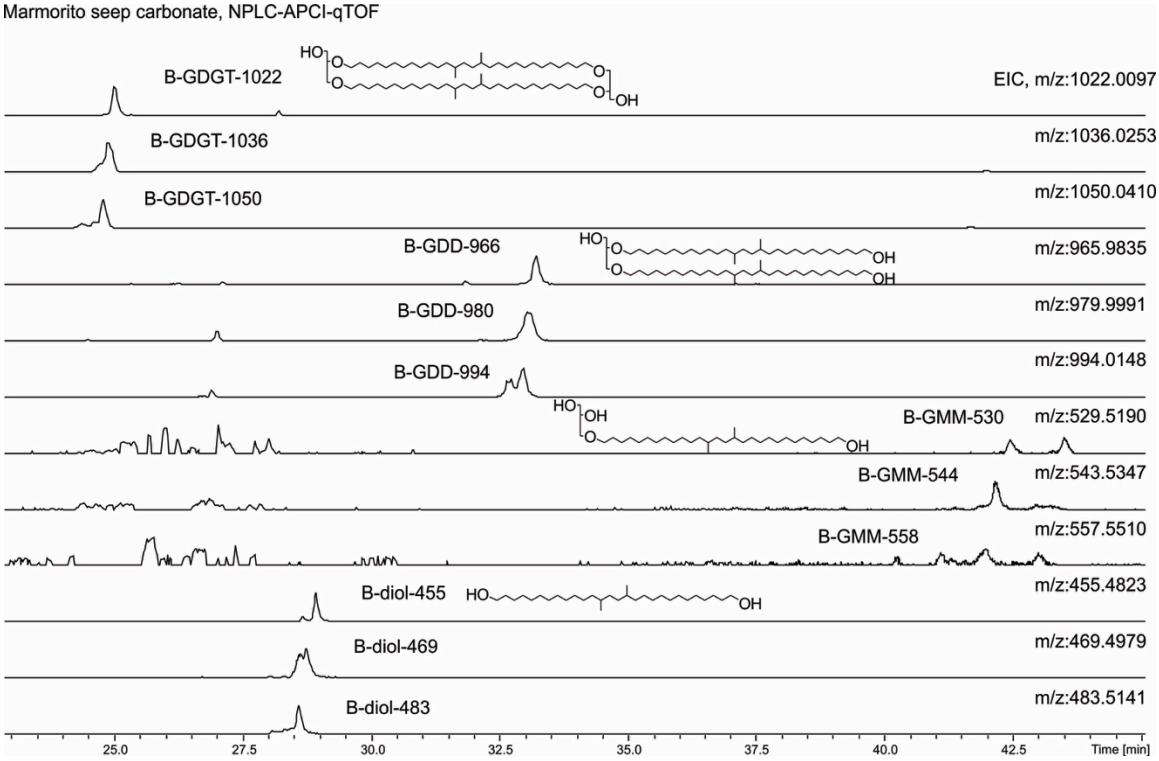

976

977 **Figure S4**

978 Extracted ion chromatograms of NPLC-APCI-qTOF showing the occurrence of branched
979 GDGTs and derivatives in Marmorito seep carbonate.

980

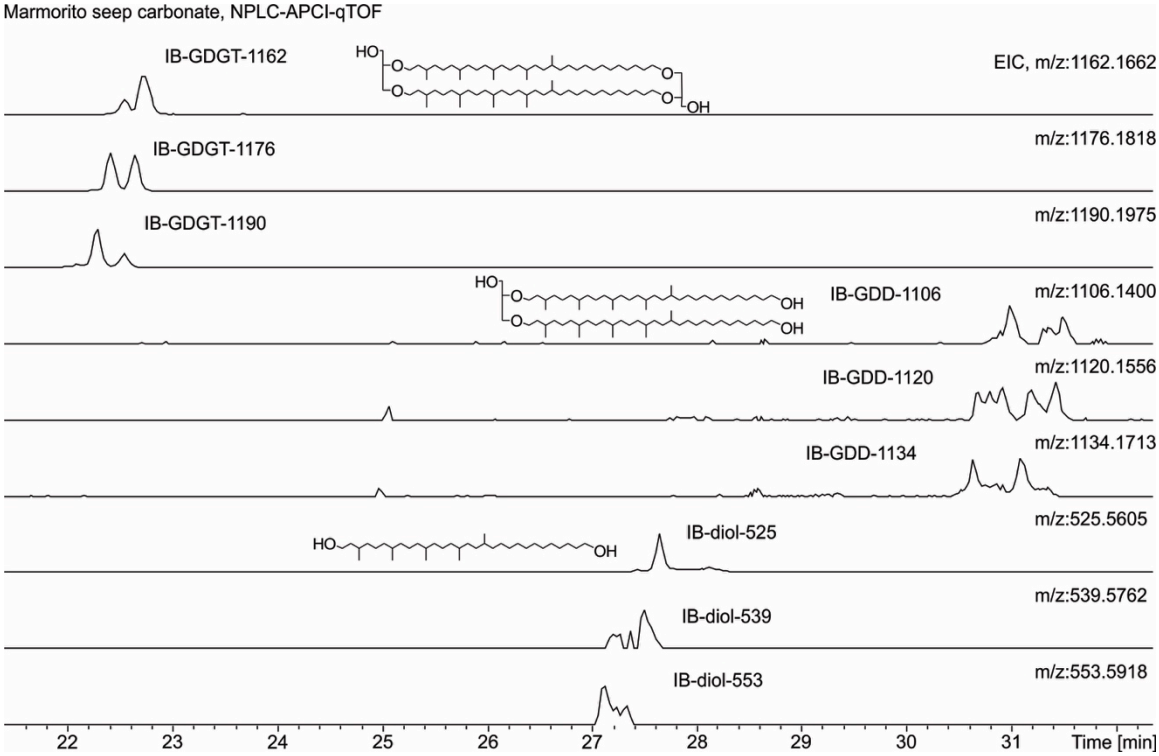

Figure S5

Extracted ion chromatograms of NPLC-APCI-qTOF showing the occurrence of IB-GDGTs and derivatives in Marmorito seep carbonate.

Table

Compounds	Abbreviation	Structural illustration	Distribution				
			Leg201-1227	Marmorito seep carbonate	Guaymas Basin 4568	Hot spring T-15	*N. maritimus* late stat. phase
glycerol dialkyl glycerol tetraether	GDGT	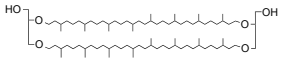	+	+	+	+	+
glycerol dialkyl glycerol triether alcohol	GDGTol	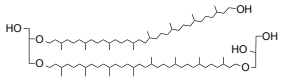	+	+	+	n.d.	+
glycerol dialkyl glycerol triether acid	GDGTA	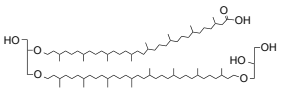	+	+	n.d.	n.d.	n.d.
glycerol dibiphytanol diether	GDD	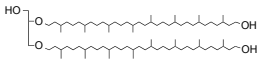	+	+	+	+	+
glycerol dibiphytanol diether monoacid	GDDA	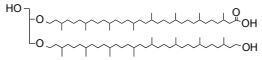	+	+	+	n.d.	+
glycerol dibiphytanol diether diacid	GDDAA	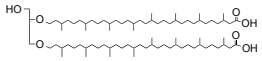	n.d.	+	n.d.	n.d.	n.d.
glycerol monobiphytanyl glycerol diether	GMGD	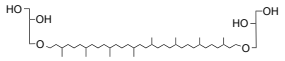	+	+	+	n.d.	n.d.
glycerol monobiphytanol monoether	GMM	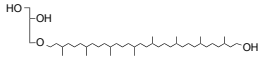	+	+	+	n.d.	n.d.
glycerol monobiphytanol monoether acid	GMMA	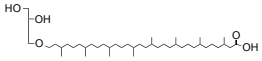	n.d.	+	n.d.	n.d.	n.d.
biphytanic diol	bpdiol	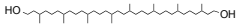	+	+	+	+	+
biphytanic monoacid	bpmonoacid/ol	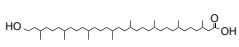	+	+	n.d.	n.d.	n.d.
biphytanic diacid	bpdiacid	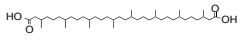	n.d.	+	n.d.	n.d.	n.d.
H-shaped glycerol monoalkyl glycerol tetraether	H-GMGT	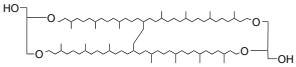	+	+	+	+	n.d.
H-shaped glycerol monoalkyl diether	H-GMD	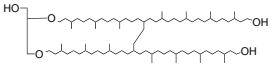	+	+	+	+	n.d.
H-shaped C_{80} tetrol	H-tetrol	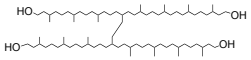	+	+	+	+	n.d.
H-shaped C_{80} monoacid	H-monoacid	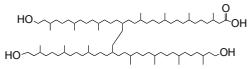	n.d.	n.d.	+	n.d.	n.d.
H-shaped C_{80} diacid	H-diacid	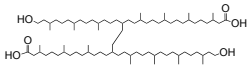	n.d.	n.d.	+	n.d.	n.d.
H-shaped C_{80} triacid	H-triacid	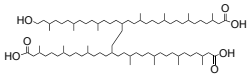	n.d.	n.d.	+	n.d.	n.d.
H-shaped C_{80} tetraacid	H-tetraacid	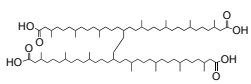	n.d.	n.d.	+	n.d.	n.d.

Figure

Click here to download high resolution image

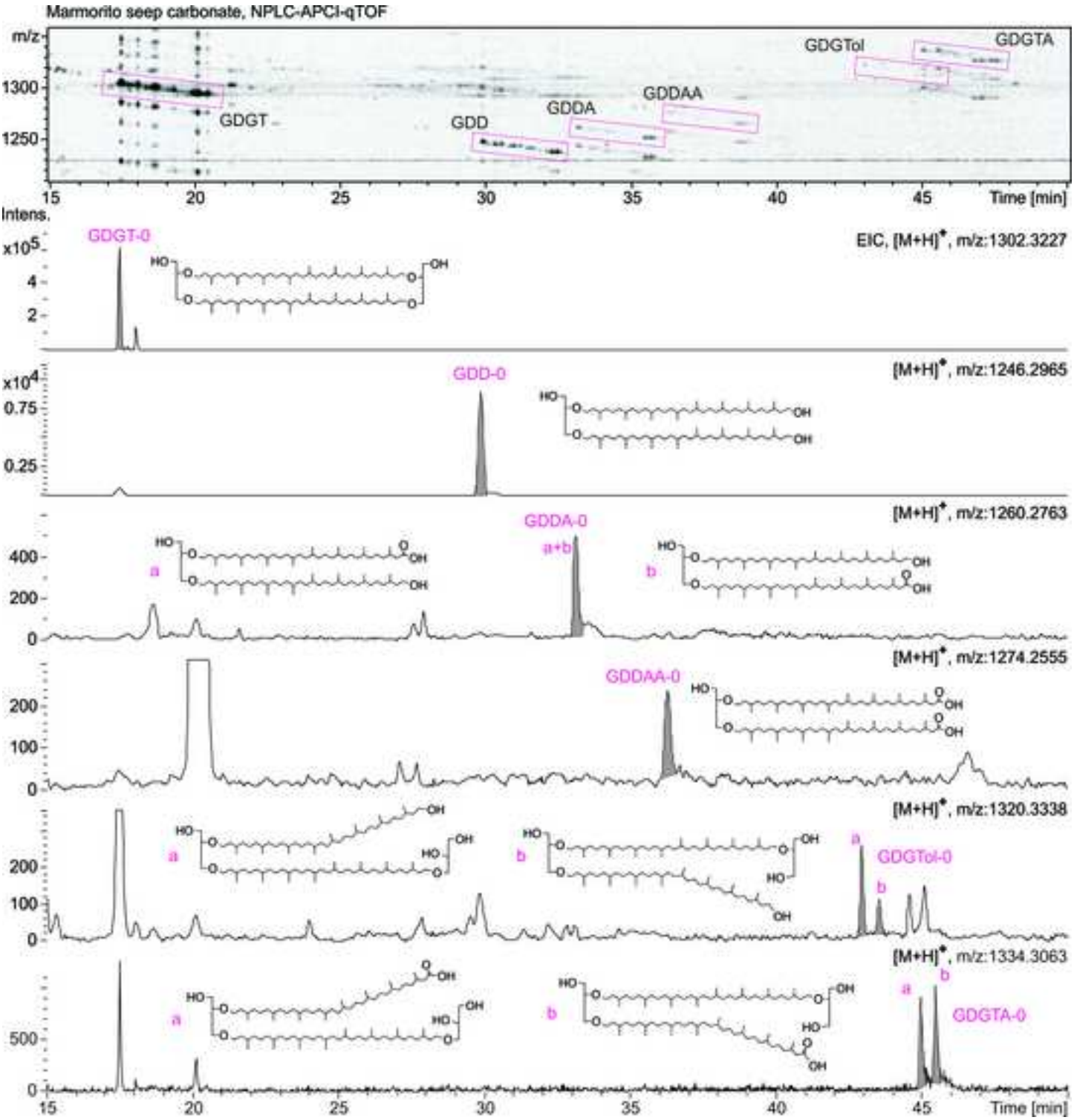

Figure

Click here to download high resolution image

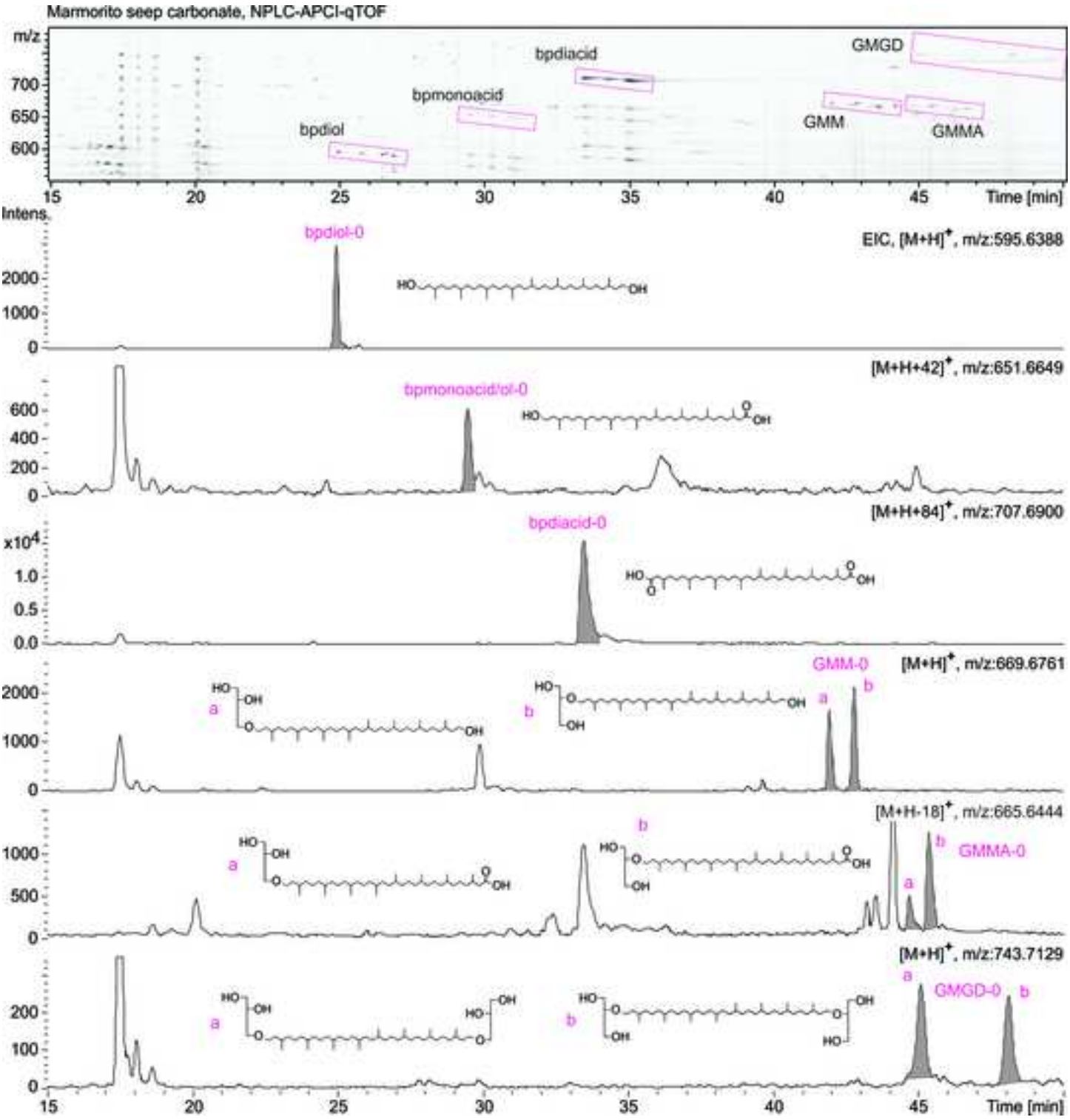

Figure

Click here to download high resolution image

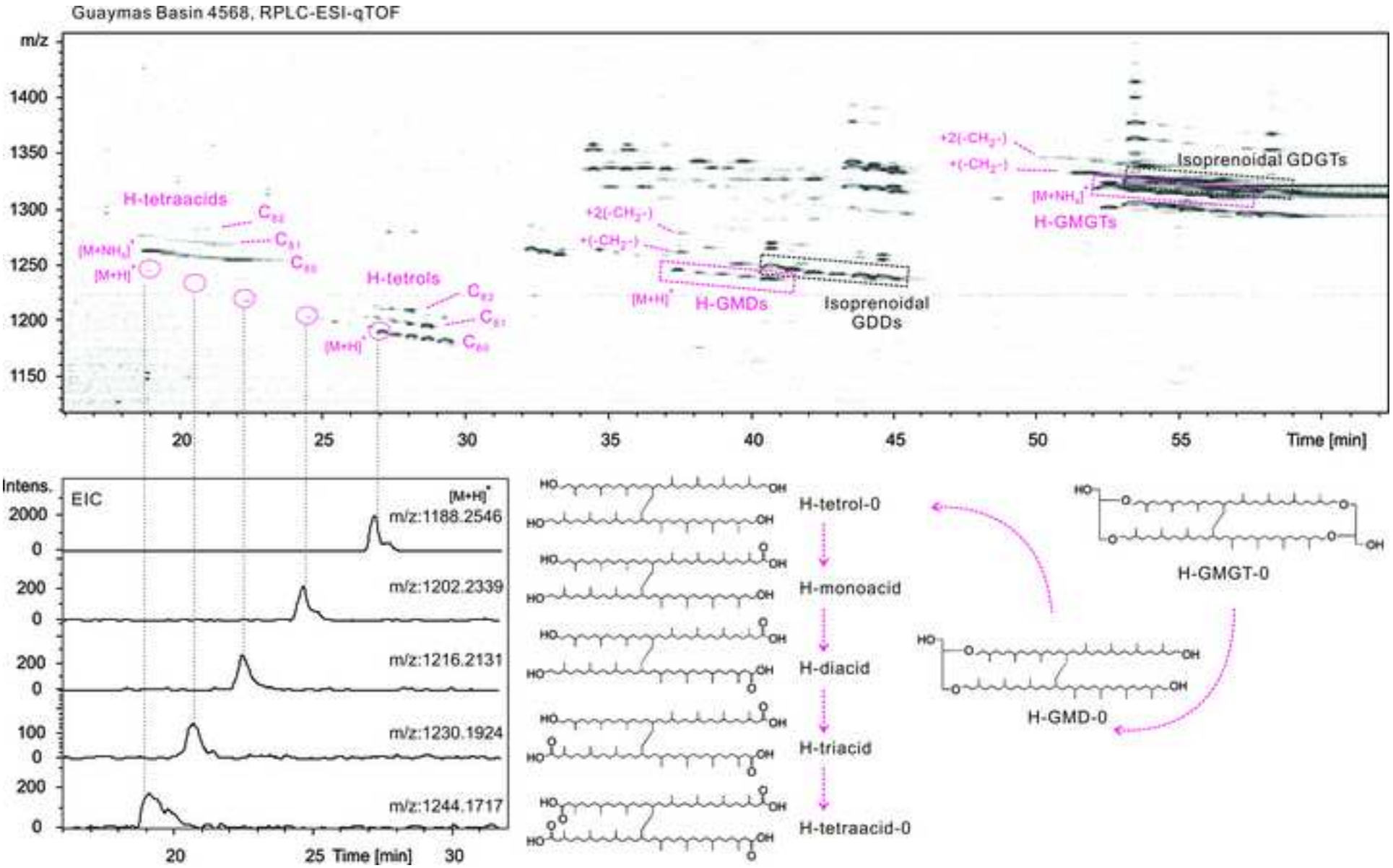

Figure
Click here to download high resolution image

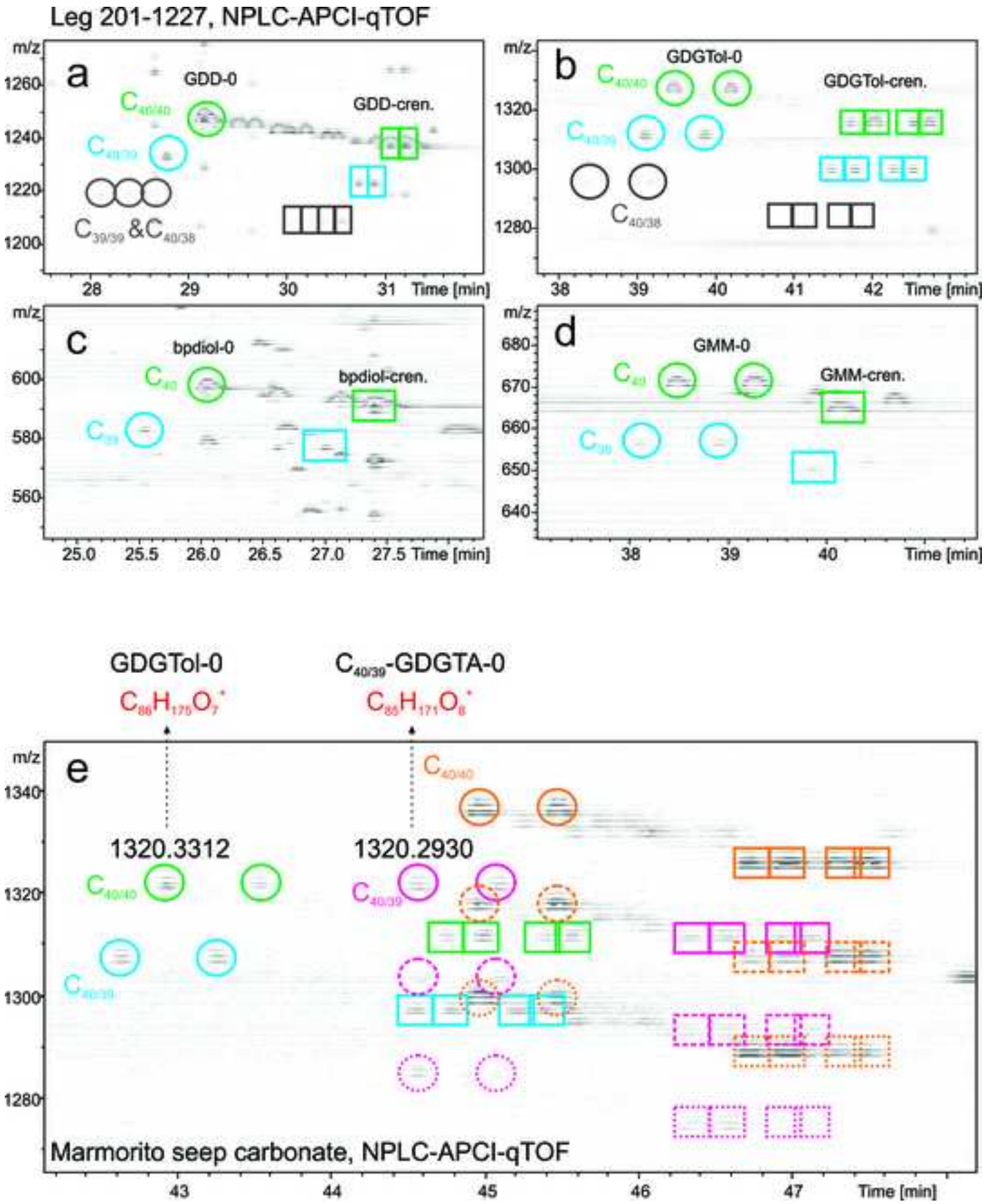

Figure
Click here to download high resolution image

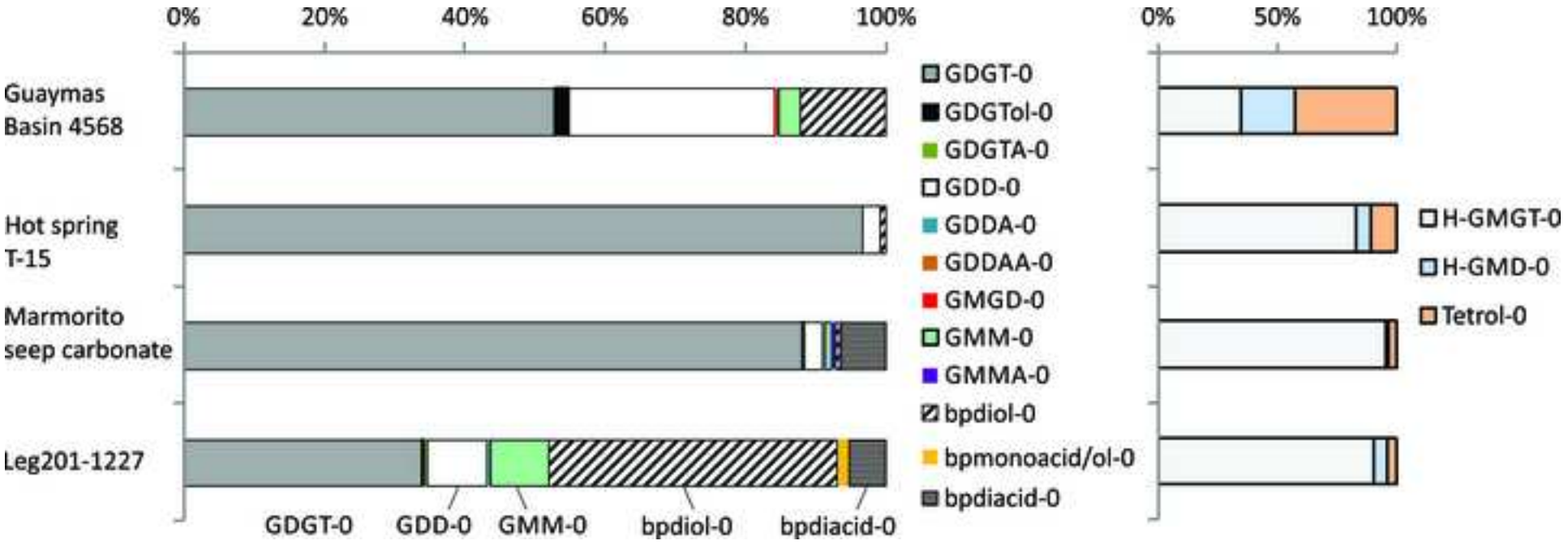

Figure
Click here to download high resolution image

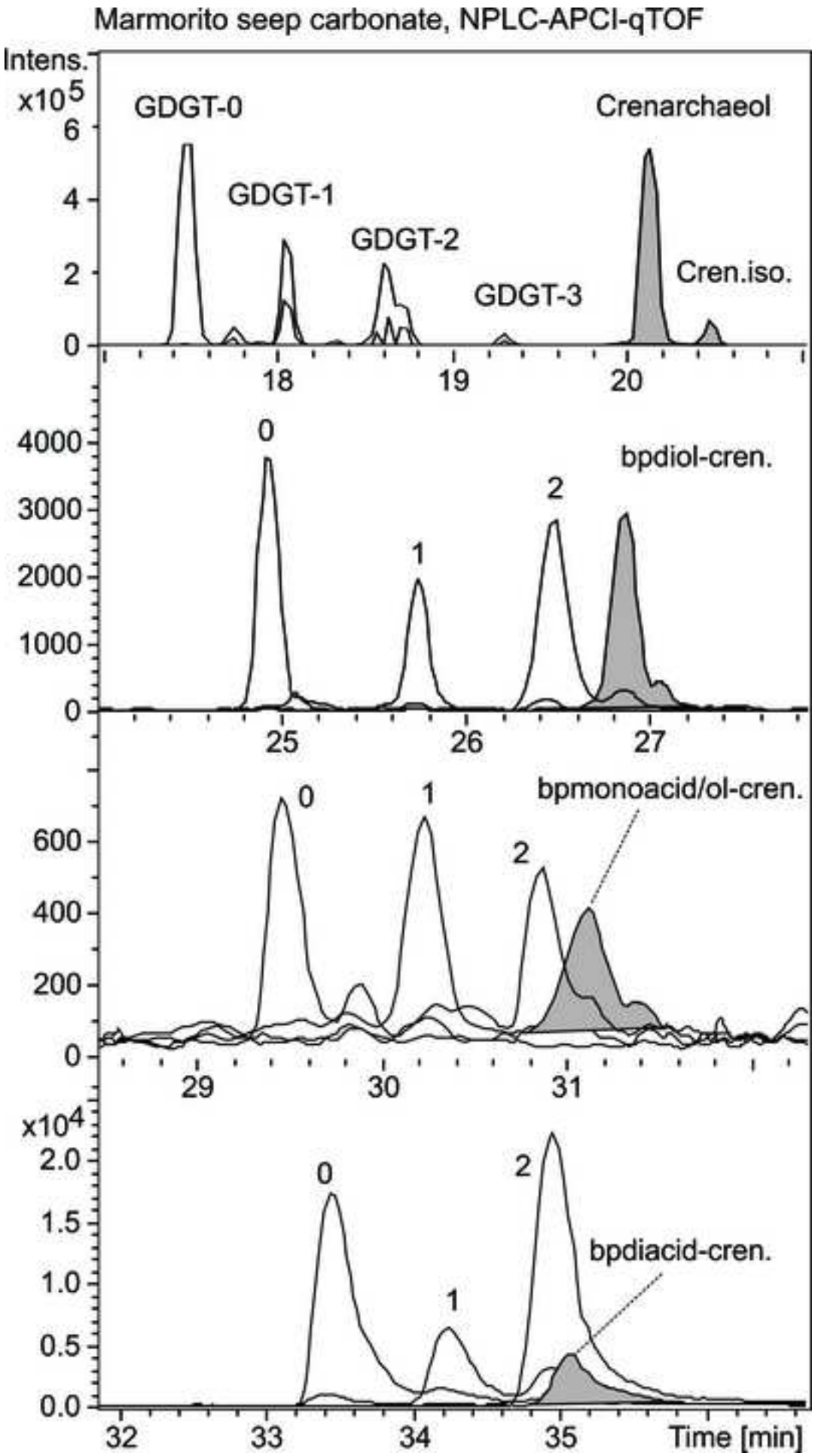

Figure

Click here to download high resolution image

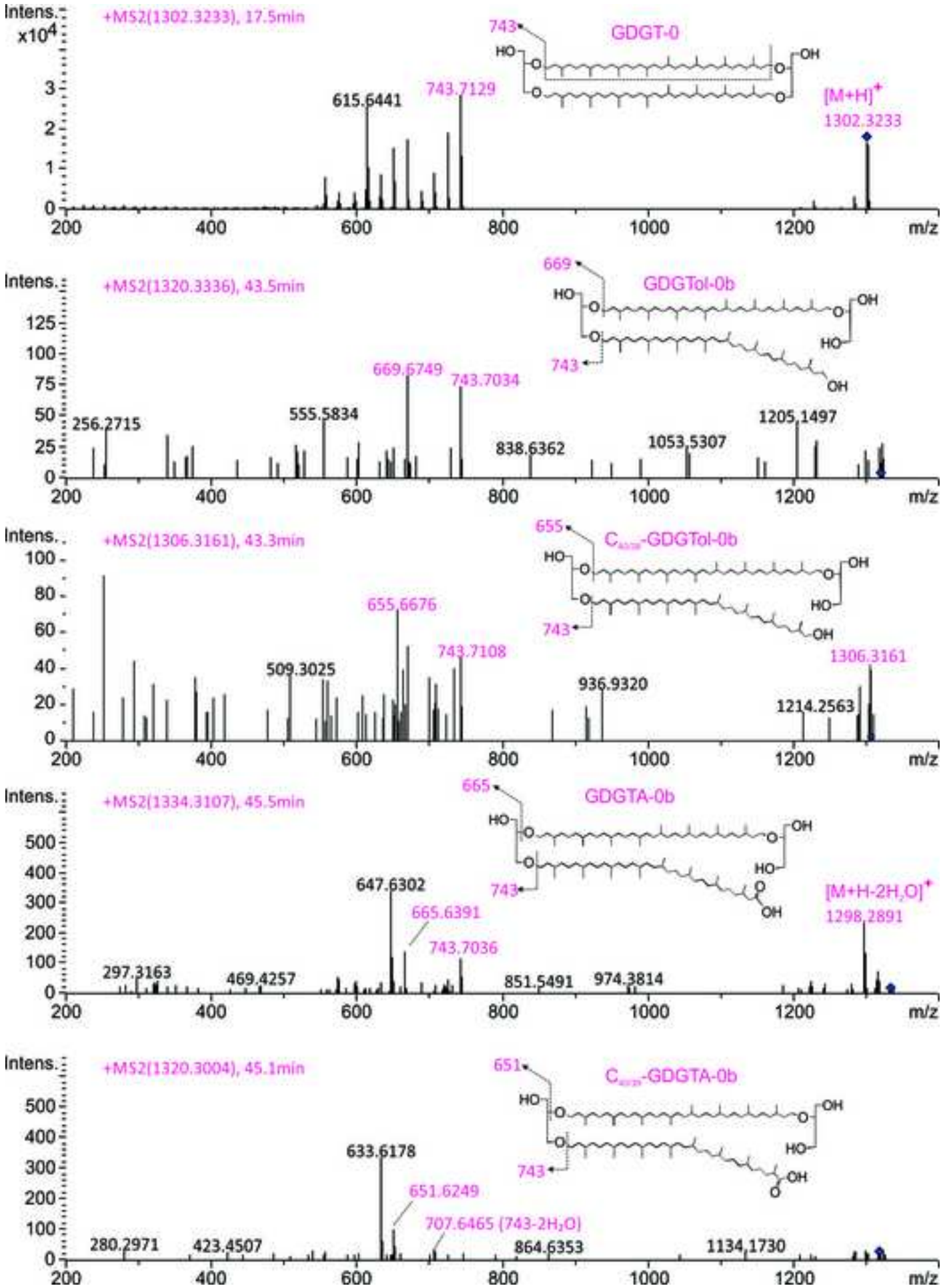

Figure

Click here to download high resolution image

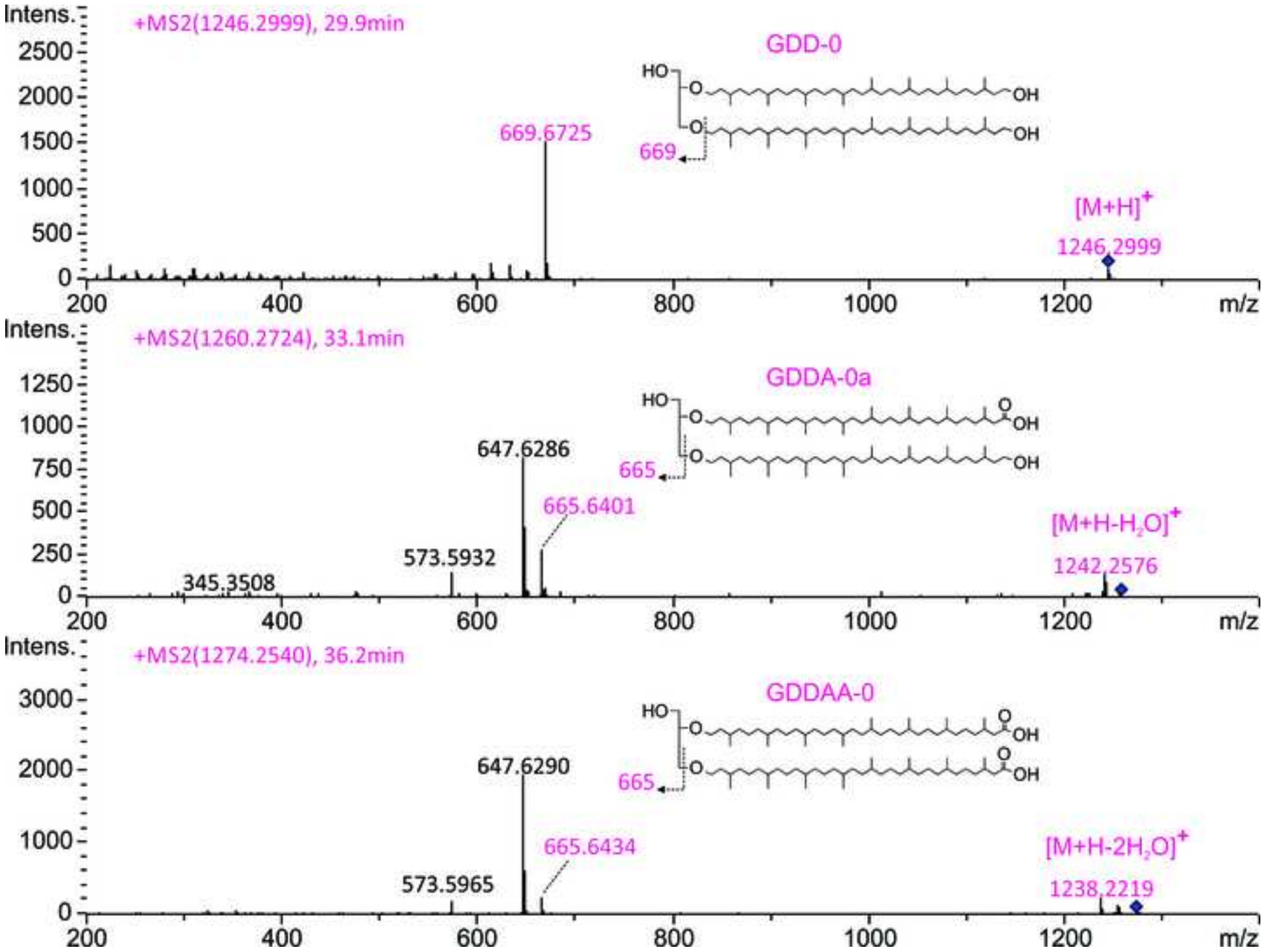

Figure

Click here to download high resolution image

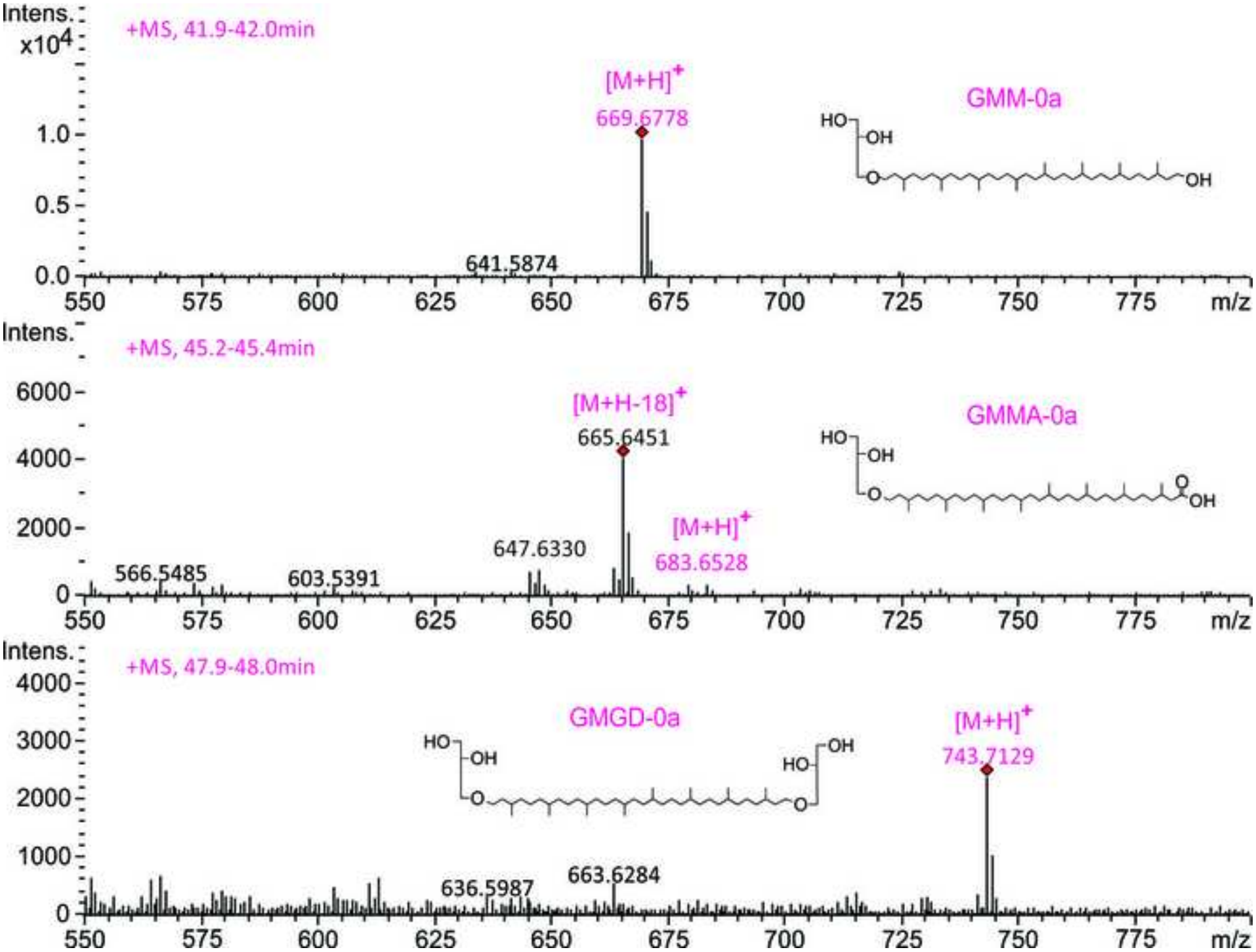

Figure

Click here to download high resolution image

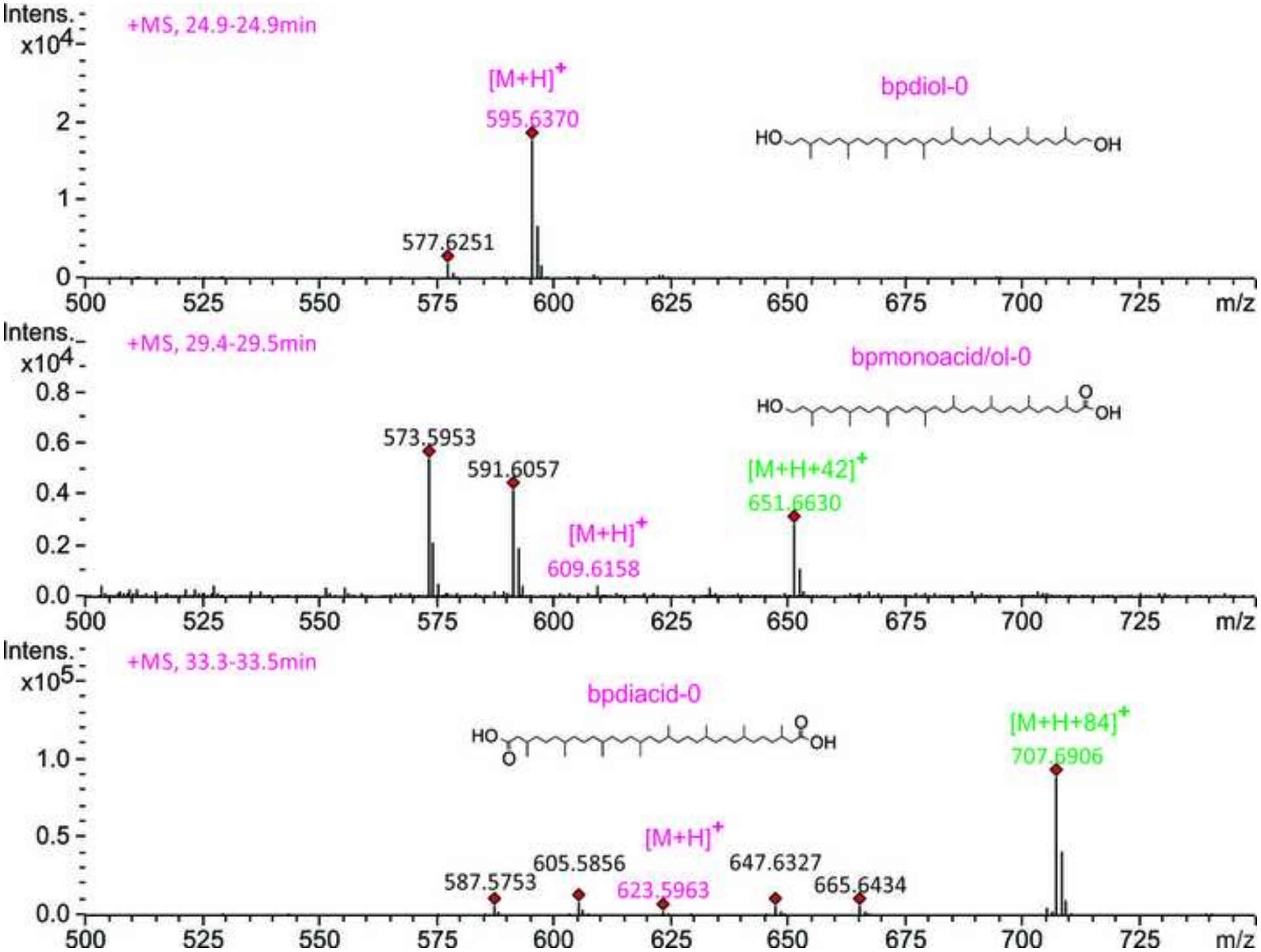

Figure

Click here to download high resolution image

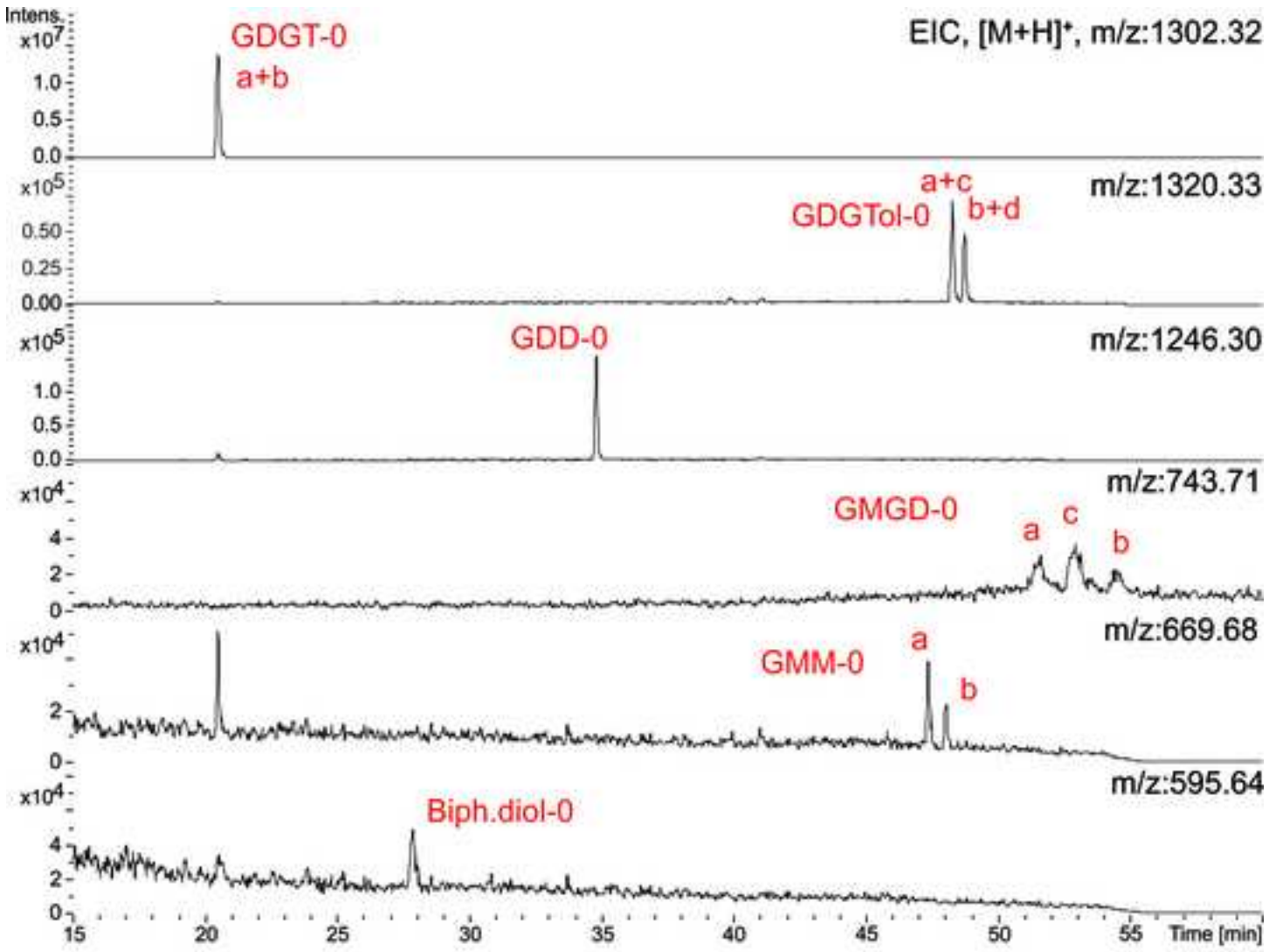

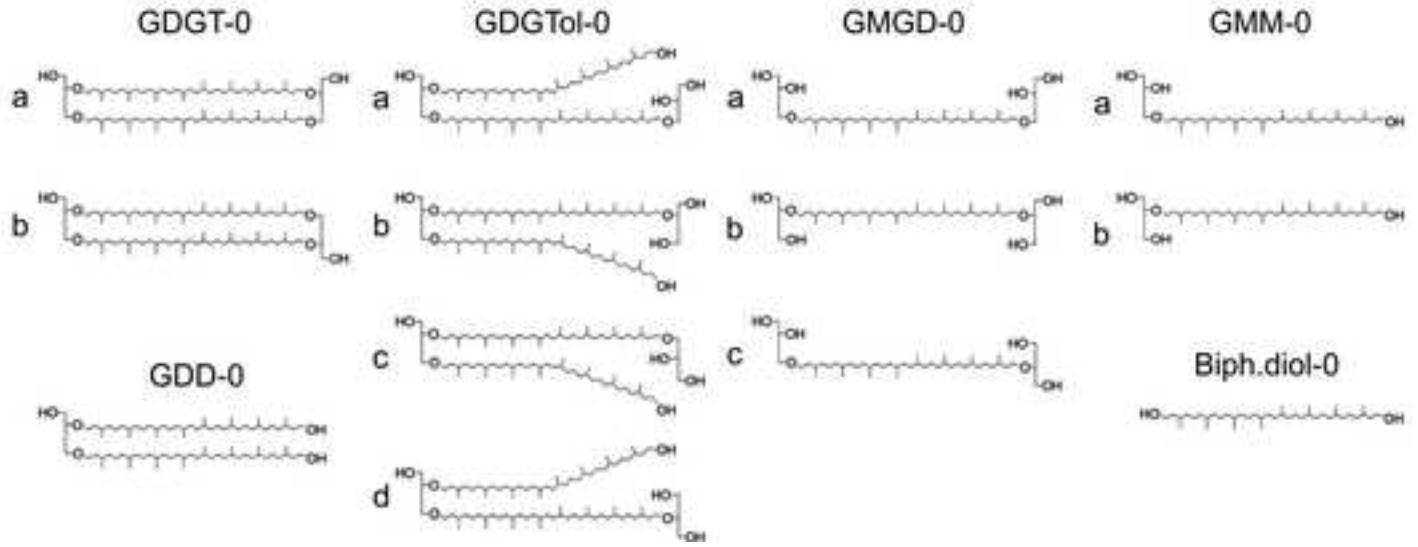

Figure

Click here to download high resolution image

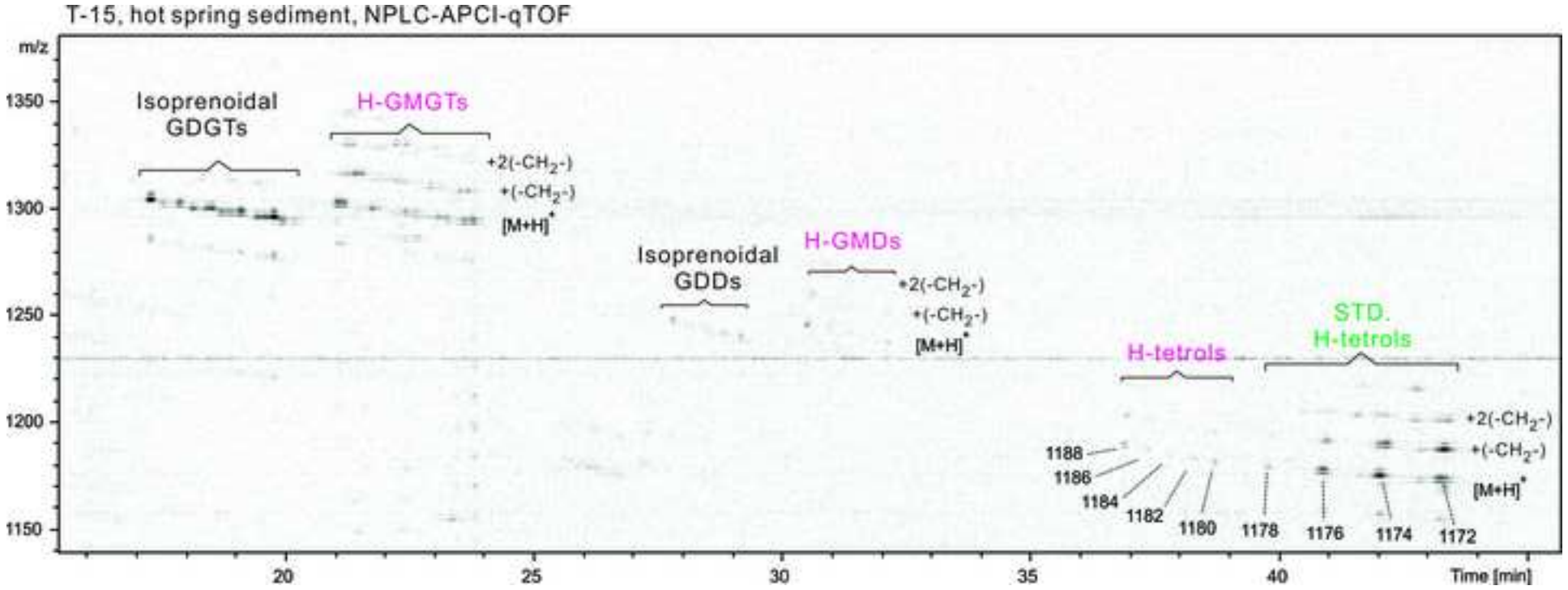

Figure
Click here to download high resolution image

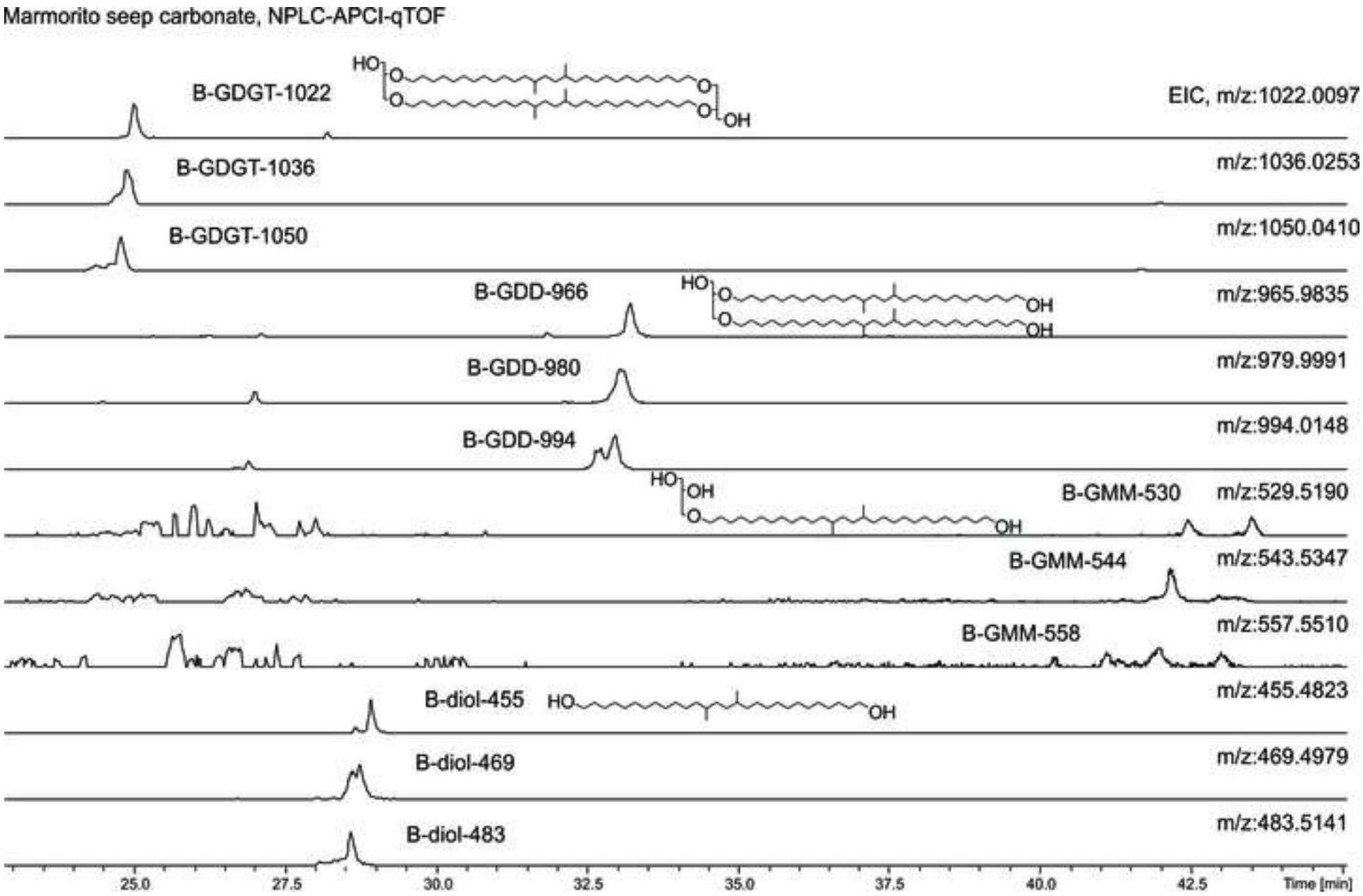

Figure
Click here to download high resolution image